

1 Dear Editor,

2

3 Thank you very much for your time and efforts regarding our manuscript. We highly appreciate  
4 the constructive comments from three reviewers that offer us the opportunity to clarify some  
5 concerns and further improve our manuscript.

6 Please find enclosed our detailed point-by-point responses to all the comments, as well as the  
7 uploaded revised version of our manuscript. The comments are black, our response in **blue**. For  
8 easy review, we have also used the "Track Changes" function in the revised manuscript to make  
9 our revisions more easily visible. The modifications are mainly threefold:

10 1. The motivation was emphasized by adding Figure 1 taken from Fan et al., PNAS 2017,  
11 showing the increase of rooting depth with the increase of HAND in most parts of hillslope.  
12 The HSC module provides a rational from an ecological perspective to understand the linkage  
13 between large-sample hillslope ecological observations and the curve of root zone storage  
14 capacity distribution (Figure 1, 2, 3)

15 2. The impact of catchment characteristics on HSC model performance was analyzed, including  
16 topography (averaged elevation, averaged HAND, averaged slope), geology (averaged depth  
17 to rock), soil texture (K factor), land use (forest cover proportion), and stream density. It was  
18 found that HSC performs better in the catchments with gentle topography, less forest cover  
19 and arid climate.

20 3. The discussion was improved, on the model comparison between HSC and TOPMODEL in  
21 the Bruntland Burn catchment.

22 We hope responses and revisions will satisfy all reviewers' comments. Thanks again and we are  
23 looking forward to receiving your decision.

24

25 Yours sincerely,

26 Hongkai Gao on behalf of all the co-authors

27

28

29

30

31

32

33

34

35 **Anonymous Referee #1**

36 accepted as is

37

38 **Anonymous Referee #2**

39 I am appreciated that the authors add more explanations and discussions to improve the manuscript.  
40 However, the benefits from the application of the new runoff generation module are still not clear to  
41 me. The authors discussed the model uncertainty in the introduction section, while the results have not  
42 addressed this issue in their manuscript. The ability of the proposed module to improve the  
43 conceptualization of real catchment behaviors in the hydrological model is not convincing. Some of  
44 other concerns are listed as follow.

45 **Reply:** We thank the Anonymous Referee #2 for his/her further comments and suggestions on the  
46 manuscript. Our detailed replies can be found below.

47

48 1. The authors defined 'calibration free' as one of the major sell points of their work. However, the  
49 benefits from the reduced calibration work need to be further interpreted in the results. After the  
50 integration of the proposed runoff generation module, the hydrological model still needs calibration.  
51 The computation cost caused by the preparation of the HAN curves is even higher than the  
52 computation cost reduced by the smaller parameter space. For the practical application of hydrological  
53 modeling, running automatic calibration without any pre-calculation is more preferable, unless the  
54 authors can provide proofs for that the new runoff generation module is more close to the realism in the  
55 catchment. Figures 6-9 compared the simulated and observed saturated areas by various modules.  
56 However, I would say the HSC module has not shown higher performance than the Topmodel in Figures  
57 8-9. The Topmodel shows higher performance at low saturated areas (Fig. 9a). Figure 6 has not  
58 evaluated the distribution of saturated areas produced by the HBV model, which can be also set up at  
59 grid scale. Figure 7 does not make any sense, considering observation is missing.

60

61 **Motivation and rational of HSC**

62 For the motivation of this study, we added a figure (Figure 1), taken from Fan et al., 2017 (with  
63 permission from PNAS), showing the increase of rooting depth with the increase of HAN in most parts  
64 of hillslope, only except for the very high HAN hillslopes. Figure 1 is the result of thousands of  
65 ecological measurements at global scale, which illustrates that the assumption of HSC likely fits well with  
66 catchment realism supported by a large dataset of field observations. The HSC module provides a  
67 rational from an ecological perspective to understand the linkage and mechanism between large-sample  
68 hillslope ecological observations and the curve of root zone storage capacity distribution (Figure 1, 2, 3).

69 The benefits of the new HSC module are two- fold. From a technical point of view, the HSC allows us to  
70 make Prediction in Ungauged Basins without calibrating the beta parameter in many conceptual  
71 hydrological models (e.g. HBV, Xinanjiang etc). But as the reviewer pointed out (which we also  
72 recognized) there are other modules with relatively parsimonious parameterizations (e.g. TOPMODEL

73 and GR4J), that can work well in terms of model performance. In contrast, the HSC module,  
74 furthermore, from a scientific point of view, provides us with a new perspective on the linkage between  
75 root zone storage capacity in both hillslopes and at catchment scales (long-term ecosystem evolution)  
76 with insights into runoff generation (event scale rainfall-runoff generation).

77 Further asking questions of “why” rather than “what” likely leads to more useful insights and a new way  
78 forward (McDonnell et al., 2007). Catchments are geomorphological and even ecological systems whose  
79 parts are inter-related due to catchment self-organization and co-evolution (Sivapalan and Blöschl,  
80 2015; Savenije and Hrachowitz, 2017).

81 **Computational cost**

82 The computational cost of the HSC is more expensive than HBV, and similar to TOPMODEL, due to the  
83 cost of preprocessed topographic analysis. But once the Su-As curve is completed, the computational  
84 cost is quite comparable with HBV.

85 **Interpretation of Figure 6**

86 For Figure 6 (now Figure 7 in the revised manuscript), we may politely disagree with the Anonymous  
87 Reviewer 2. The HBV cannot generate the distribution of saturated areas at catchment scale. Since HBV  
88 only calculates the runoff coefficient of certain rainfall events in a lumped way. It cannot map out the  
89 saturated area variation. We think it is still worthwhile to compare the contributing area simulated by  
90 the new HSC module and the TOPMODEL, since TOPMODEL is a benchmark in this study. Also, it might  
91 be interesting to show the simulated contributing area compared to the observed saturated area,  
92 despite that they are not exactly the same. In theory, the observed saturated area should be within the  
93 simulated contributing area, due to the fact that the saturated soil moisture is always larger than field  
94 capacity. From this point of view, we show that the observed saturated area is almost always within the  
95 contributing area simulated by HSC, but TOPMODEL missed this important feature (July 2 and  
96 September 2 in 2008) supporting our statement that HSC performed better in reproducing saturated  
97 area variation.

98 We rephrased the discussion on model comparison between HSC and TOPMODEL. More details can be  
99 found in Line 427-430, 666-668 in the revised manuscript (clear version hereinafter).

100

101 2. The comparable or better performance produced by the model coupled with the proposed  
102 runoff generation module may be caused by either the application of the new runoff generation module  
103 or the calibration run with less parameters. The automatic calibration algorithm could produce higher  
104 performance when the calibration parameter space is reduced. This need to be further analyzed.

105 **New module or less parameter?**

106 This is indeed a very good point. Parsimonious models (e.g. the GR4J, ref. Perrin et al., 2003), with  
107 empirical curves similar to the HSC, likely result in good model performance. Parameter identifiability in  
108 calibration is one of the reasons. However, the rationale of most models is still largely unknown, and  
109 lack of the physically explanation to interpret these empirical curves described by mathematical  
110 functions (e.g. Equation 3 in Perrin et al., 2003). (Line 576-580).

111

112 3. The motivation of this sturdy is not clear enough. With the proposed module, more calculation  
113 work is needed and produced the same or bit better model performance. The model uncertainty has not  
114 been analyzed, and the transferability of the runoff generation module has not been investigated in this  
115 study.

116 In general, limitations in the current work certainly prevented more scientific contributions from this  
117 study. The authors should pay more efforts to make their motivation and results more convincing.

## 118 **Motivation**

119 The motivation can be found in our reply to the first comment and with all due respect the Reviewer  
120 does seem to miss the main point, which we tried to further emphasize in the revised manuscript: Since  
121 the HSC is an a priori module, which we do not calibrate, the module can be perfectly “transferred” to  
122 other catchments without calibration. Hence, the large sample application!

123

124

## 125 **Anonymous Referee #3**

126 I would like to thank the authors for their revision, particularly improving discussion section. For some of  
127 my comments, however, I do not see a clear response:

128 1) I'm still not convinced by the use of BB basin to support the conclusion that the new model  
129 (HSC) outperforms the TOPMODEL (“We found that the HSC performed better in reproducing the spatio-  
130 temporal pattern of the observed saturated areas in the BB compared to TOPMODEL”). The Figures 6  
131 and 8 clearly indicate that both models are significantly overestimating what is considered as ground  
132 truth here (observed pattern of saturated area). I do not understand well the argument that the values  
133 are not directly comparable. If so, why to compare them? This part is not well linked with the validation  
134 of the new approach in its current form.

135 Thank you for your comment, which we tried to clarify in our revised manuscript. We have rephrased  
136 the statements in Section 4.3 and Line 640-644.

## 137 **Section 4.3:**

138 Comparing the estimated contributing area of TOPMODEL with the HSC module, we found the results of  
139 the HSC correlates better ( $R^2=0.60$ ,  $IKGE=-3.0$ ) with the observed saturated areas than TOPMODEL  
140 ( $R^2=0.50$ ,  $IKGE=-3.4$ ) (Figure 10). For spatial patterns, the HSC contributing area is located close to the  
141 river network, and reflects the spatial pattern of observed saturated area. While TOPMODEL results are  
142 more scattered, probably due to the sensitivity of TWI to DEM resolution (Figure 7). The HSC is more  
143 discriminating in terms of less frequently giving an unrealistic 100% catchment saturation retaining parts  
144 of the unsaturated upper hillslopes.

## 145 **Line 640-644:**

146 Interestingly, in theory the observed saturated area should be within the simulated contributing area,  
147 due to the fact that the saturated soil moisture is always larger than field capacity. From this point of

148 view, the observed saturated area is smaller and within the contributing area simulated by HSC, but  
149 TOPMODEL missed this important feature.

150

151 2) In some places of section 5, it will be interesting to see more specific interpretation of the  
152 results. E.g. for statement “Figure 11c interestingly shows that in some catchments, there is almost no  
153 threshold...” it will interesting to see some more specific generalisation for which catchments it applies.  
154 Or “...where the HSC model performed better are mostly located in the Great Plains, with modest  
155 sloping (4.0 degree)...” Does it apply/relate to all catchments with slope 4degree or even less (“HSC  
156 outperformed catchments have flat terrain (2.3 degree) with moderate averaged HAND value (26m)”)?  
157 Some more evaluations (or more specific formulations) allowing some more specific generalisation of  
158 results will be interesting here. Where one can expect the new model is better/worser than  
159 TOPMODEL/HBV in other regions – outside US?

160 This is an excellent question, thank you, which helped us to improve the presentation of this work. We  
161 did a systematic analysis between model performance and catchment characteristics included in the  
162 revised manuscript. See Line 494-505, and the new Table 3 and Table 4.

163

164 3) Figure 6 legend is still confusing for me. Would it be possible to make all three  
165 columns/methods of maps just with binary colours (is/is not saturated)?

166 Thank you. This was changed in the revised manuscript.

167

168 4) Please add the new references to the list.

169 Done.

170

171

172

173

174

175

176

177

178

179

180

181 A simple topography-driven and  
182 calibration-free runoff generation module

183 Hongkai Gao<sup>1,2,3 \*</sup>, Christian Birkel<sup>4,5</sup>, Markus Hrachowitz<sup>6</sup>, Doerthe Tetzlaff<sup>5</sup>, Chris Soulsby<sup>5</sup>, Hubert H. G. Savenije<sup>6</sup>

184

185 <sup>1</sup> Key Laboratory of Geographic Information Science (Ministry of Education of China), East China Normal University,  
186 Shanghai, China.

187 <sup>2</sup> School of Geographical Sciences, East China Normal University, Shanghai, China.

188 <sup>3</sup> Julie Ann Wrigley Global Institute of Sustainability, Arizona State University PO Box 875402. Tempe, AZ 85287-5402.

189 <sup>4</sup> Department of Geography, University of Costa Rica, San José, Costa Rica

190 <sup>5</sup> Northern Rivers Institute, University of Aberdeen, Scotland.

191 <sup>6</sup> Water Resources Section, Delft University of Technology, Delft, Netherlands.

192

193 \*Corresponding to Hongkai Gao (hkgao@geo.ecnu.edu.cn)

194

195 **Abstract**

196 Reading landscapes and developing calibration-free runoff generation models that adequately reflect land  
197 surface heterogeneities remains the focus of much hydrological research. In this study, we report a novel  
198 and simple topography-driven runoff generation parameterization – the HAND-based Storage Capacity  
199 curve (HSC), that uses a topographic index (HAND, Height Above the Nearest Drainage) to identify  
200 hydrological similarity and the extent of saturated areas in catchments. The HSC can be used as a module  
201 in any conceptual rainfall-runoff model. Further, coupling the HSC parameterization with the Mass Curve  
202 Technique (MCT) to estimate root zone storage capacity ( $S_{u\text{Max}}$ ), we developed a calibration-free runoff  
203 generation module HSC-MCT. The runoff generation modules of HBV and TOPMODEL were used for  
204 comparison purposes. The performance of these two modules (HSC and HSC-MCT) was first checked  
205 against the data-rich Bruntland Burn (BB) catchment in Scotland, which has a long time series of field-  
206 mapped saturation area extent. We found that ~~the HSC, HBV and TOPMODEL all perform well in~~ to ~~reproducing~~ ~~reproduce~~ ~~the~~ ~~the spatio-temporal pattern of the observed saturated areas in the~~ ~~BBhydrograph, but the HSC module performs better into~~ ~~reproducing~~ ~~the~~ ~~saturated area variation, in terms~~

209 of correlation coefficient and spatial patterns compared to TOPMODEL. The HSC and HSC-MCT modules  
210 were subsequently tested for 323 MOPEX catchments in the US, with diverse climate, soil, vegetation and  
211 geological characteristics. Comparing with HBV and TOPMODELIn comparison with HBV and TOPMODEL,  
212 the HSC performs better in both calibration and validation, particularly especially in the catchments with  
213 gentle topography, less forest cover and arid climate. Despite having no calibrated parameters, the HSC-  
214 MCT module performed comparably well with calibrated modules, highlighting the robustness of the HSC  
215 parameterization to describe the spatial distribution of the root zone storage capacity and the efficiency  
216 of the MCT method to estimate  $S_{u\text{Max}}$ . Moreover, the HSC module facilitated visualization of the saturated  
217 area, which has the potential to be used for broader hydrological, ecological, climatological,  
218 geomorphological, and biogeochemical studies. This novel and calibration-free runoff generation module  
219 helps to improve parameterization will benefit the Prediction in Ungauged Basins, and has great  
220 potential to be generalized at the global scale.

221

## 222 1 Introduction

223 Determining the volume and timing of runoff generation from rainfall inputs remains a central challenge  
224 in rainfall-runoff modelling (Beven, 2012; McDonnell, 2013). Creating a simple, calibration-free, but robust  
225 runoff generation module has been, and continues to be, an essential pursuit of hydrological modellers.  
226 Although we have made tremendous advances to enhance our ability on Prediction in Ungauged Basins  
227 (PUB) (Sivapalan et al., 2003; Blöschl et al., 2013; Hrachowitz et al., 2013), it is not uncommon that models  
228 become increasingly complicated in order to capture the details of hydrological processes shown by  
229 empirical studies (McDonnell, 2007; Sivapalan, 2009; Yu et al., 2014). More detailed process  
230 conceptualization normally demands higher data requirements than our standard climatological and  
231 hydrological networks can provide, leading to more calibrated parameters and a probable increase in  
232 model uncertainty (Sivapalan, 2009).

233 Hydrological connectivity is a key characteristic of catchment functioning, controlling runoff generation.  
234 It is a property emerging at larger scales, describing the temporal dynamics of how spatially  
235 heterogeneous storage thresholds in different parts of catchments are exceeded to contribute to storm  
236 runoff generation and how they are thus “connected to the stream” (e.g. Zehe and Blöschl, 2004;  
237 Bracken and Croke, 2007; Lehmann et al., 2007; Zehe and Sivapalan, 2009; Ali et al., 2013; Blume and  
238 van Meerveld, 2015). Connectivity is controlled by a multitude of factors (Ali and Roy, 2010), including

239 but not limited to surface (e.g. Jencso et al., 2009) and subsurface topography (e.g. Tromp-van Meerveld  
240 and McDonnell, 2006), soils (including preferential flow networks; e.g. Zehe et al., 2006; Weiler and  
241 McDonnell, 2007), and land cover (e.g. Imeson and Prinsen, 2004; Jencso and McGlynn, 2011; Emanuel  
242 et al., 2014), but also by the wetness state of the system (e.g. Detty and McGuire, 2010; Penna et al.,  
243 2011; McMillan et al., 2014; Nippgen et al., 2015).

244 In detailed distributed hydrological bottom-up models, connectivity emerges from the interplay of  
245 topography, soil type and water table depth. For example, TOPMODEL (Beven and Kirkby, 1979; Beven  
246 and Freer, 2001) uses topographic wetness index (TWI) to distinguish hydrologic similarity; and SHE  
247 (Abbott et al. 1986) and tRIBS (Ivanov et al. 2004; Vivoni et al. 2005) use partial differential equations to  
248 describe the water movement based on pressure gradients obtained by topography; and the  
249 Representative Elementary Watershed (REW) approach divides catchment into a number of REWs to  
250 build balance and constitutive equations for hydrological simulation (Reggiani et al., 1999; Zhang and  
251 Savenije, 2005; Tian et al., 2008). As the relevant model parameters such as local topographic slope and  
252 hydraulic conductivity can, in spite of several unresolved issues for example relating to the differences in  
253 the observation and modelling scales (e.g. Beven, 1989; Zehe et al., 2014), be obtained from direct  
254 observations, they could *in principle* be applied without calibration.

255 Zooming out to the macro-scale, top-down models, in contrast, are based on emergent functional  
256 relationships that integrate system-internal heterogeneity (Sivapalan, 2005). These functional  
257 relationships require parameters that are effective on the modelling scale and that can largely not be  
258 directly determined with small-scale field observations (cf. Beven, 1995), thus traditionally determined  
259 by calibration. However, frequently the number of observed variables for model calibration is, if  
260 available at all, limited to time series of stream flow. The absence of more variables to constrain models  
261 results in such models being ill-posed inverse problems. Equifinality in parameterization and in the  
262 choice of parameters then results in considerable model uncertainty (e.g. Beven, 1993, 2006). To limit  
263 this problem and to also allow predictions in the vast majority of ungauged catchments, it is therefore  
264 desirable to find ways to directly infer effective model parameters at the modelling scale from readily  
265 available data (Hrachowitz et al., 2013).

266 The component that is central for establishing connectivity in most top-down models is the soil moisture  
267 routine. Briefly, it controls the dynamics of water storage and release in the unsaturated root zone and  
268 partitions water into evaporative fluxes, groundwater recharge and fast lateral storm flow generating  
269 runoff (Gao et al., 2018a; Shao et al., 2018). The latter of which is critical from the aspect of connectivity.

270 In majority regions, Hortonian overland flow (HOF, i.e. infiltration excess overland flow) is of minor  
271 importance (Dunne and Black, 1970; Sklash and Farvolden, 1979; Beven, 2004; Burt and McDonnell,  
272 2015), even in arid regions where often most locally generated HOF is re-infiltrated while flowing on  
273 hillslopes (Liu et al., 2012) and never reaches the stream channel network. Thus the term saturation  
274 excess flow (SEF) can represent, depending on the model and the area of application, different  
275 processes, such as saturation overland flow, preferential flow, flow through shallow, high permeability  
276 soil layers or combinations thereof. The interplay between water volumes that are stored and those that  
277 are released laterally to the stream via fast, connected flow paths (“connectivity”) is in most top-down  
278 models described by functions between water stored in the unsaturated root zone (“soil moisture”) and  
279 the areal proportion of heterogeneous, local storage thresholds that are exceeded and thus  
280 “connected” (Zhao et al., 1980). In other words, in those parts of a catchment where the storage  
281 threshold is exceeded will generate lateral flows, and can alternatively be interpreted as runoff  
282 coefficient (e.g. Ponce and Hawkins, 1996; Perrin and Andreassian, 2001; Fenicia et al., 2007; Bergström  
283 and Lindström, 2015). Thus the idea goes back to the variable contributing area concept, assuming that  
284 only partial areas of a catchment, where soils are saturated and thus storage thresholds are exceeded,  
285 contribute to runoff (Hewlett, 1961; Dunne and Black, 1970; Hewlett and Troendle, 1975). Although  
286 originally developed for catchments dominated by saturation overland flow, the extension of the  
287 concept to subsurface connectivity, posing that surface and subsurface connectivity are “two sides of  
288 the same coin” (McDonnell, 2013), proved highly valuable for models such as Xinanjiang (Zhao et al.,  
289 1980), HBV (Bergström and Forsman, 1973; Bergström and Lindström, 2015), SCS-CN (Ponce and  
290 Hawkins, 1996; Bartlett et al., 2016), FLEX (Fenicia et al., 2008) and GR4J (Perrin and Andreassian et al.,  
291 2001).

292 Among these models, connectivity is formulated in a general form as  $C_R = f(S_u(t), S_{uMax}, \beta)$ , where  $C_R$  is the  
293 runoff coefficient, i.e. the proportion of the catchment generating runoff,  $S_u(t)$  is the catchment water  
294 content in the unsaturated root zone at any time  $t$ ,  $S_{uMax}$  is a parameter representing the total storage  
295 capacity in the unsaturated root zone and  $\beta$  is a shape parameter, representing the spatial distribution  
296 of heterogeneous storage capacities in the unsaturated root zone. The parameters of these functions  
297 are typically calibrated. In spite of being the core component of soil moisture routines in many top-down  
298 models, little effort was previously invested to find ways to determine the parameters at the catchment-  
299 scale directly from available data. An important step towards understanding and quantifying  
300 connectivity pattern directly based on observations was recently achieved by intensive experimental  
301 work in the Tenderfoot Creek catchments in Montana, US. In their work Jencso et al. (2009) were able to

302 show that connectivity of individual hillslopes in their headwater catchments is highly related to their  
303 respective upslope accumulated areas. Using this close relationship, [Smith et al. \(2013\)](#) successfully  
304 developed a simple top-down model with very limited need for calibration, emphasizing the value of  
305 “enforcing field-based limits on model parameters” ([Smith et al., 2016](#)). Based on hydrological landscape  
306 analysis, FLEX-Topo model ([Savenije, 2010](#)) can dramatically reduce the need for calibration ([Gharari et](#)  
307 [al., 2014](#)), and hold considerable potential for spatial model transferability without the need for  
308 parameter re-calibration ([Gao et al., 2014a](#); [H. Gao et al., 2016](#)). In a recent development, several  
309 studies suggest that  $S_{uMax}$  can be robustly and directly inferred long term water balance data, by the  
310 Mass Curve Technique (MCT), without the need for further calibration ([Gao et al., 2014](#); [de Boer-Euser](#)  
311 [et al., 2016](#); [Nijzink et al., 2016](#)). This leaves shape parameter  $\beta$  as the only free calibration parameter  
312 for soil moisture routines of that form. Topography is often the dominant driver of water movement  
313 caused by prevailing hydraulic gradients. More crucially, topography usually provides an integrating  
314 indicator for hydrological behavior, since topography is usually closely related with other landscape  
315 elements, such as soil vegetation climate and even geology ([Seibert et al., 2007](#); [Savenije, 2010](#); [Rempe](#)  
316 [and Dietrich, 2014](#); [Gao et al., 2014b](#); [Maxwell and Condon, 2016](#); [Gomes, 2016](#)). The Height Above the  
317 Nearest Drainage (HAND; [Rennó et al., 2008](#); [Nobre et al., 2011](#); [Gharari et al., 2011](#)), which can be  
318 computed from readily available digital elevation models (DEM), could potentially provide first order  
319 estimates of groundwater depth, as there is some experimental evidence that with increasing HAND,  
320 groundwater depths similarly increase (e.g. [Haria and Shand, 2004](#); [Martin et al., 2004](#); [Molenat et al.,](#)  
321 [2005, 2008](#); [Shand et al., 2005](#); [Condon and Maxwell, 2015](#); [Maxwell and Condon, 2016](#)). HAND can be  
322 interpreted as a proxy of the hydraulic head and is thus potentially more hydrologically informative than  
323 the topographic elevation above sea level ([Nobre et al., 2011](#)). Compared with the TWI in TOPMODEL,  
324 HAND is an explicit measure of a physical feature linking terrain to water related potential energy for  
325 local drainage ([Nobre et al., 2011](#)). More interestingly, topographic structure emerges as a powerful  
326 force determining rooting depth under a given climate or within a biome ([Figure 1](#)), revealed by a global  
327 synthesis of 2,200 root observations of >1000 species ecological observations in global scale ([Fan et al.,](#)  
328 [2017](#)). This leads us to think from ecological perspective to use the topographic information as an  
329 indicator for root zone spatial distribution without calibrating the  $\beta$ , and coupling it with the MCT  
330 method to estimate the  $S_{uMax}$ , eventually create a calibration-free runoff generation module.  
  
331 In this study we are therefore going to test the hypotheses that: (1) HAND can be linked to the spatial  
332 distribution of storage capacities and therefore can be used to develop a new runoff generation module  
333 (HAND-based Storage Capacity curve, i.e. HSC); (2) the distribution of storage capacities determined by

334 HAND contains different information than the topographic wetness index; (3) the HSC together with water  
335 balance-based estimates of  $S_{uMax}$  (MCT method) allow the formulation of calibration-free  
336 parameterizations of soil moisture routines in top-down models directly based on observations. All these  
337 hypotheses will be tested firstly in a small data-rich experimental catchment (the Bruntland Burn  
338 catchment in Scotland), and then apply the model to a wide range of larger MOPEX catchments (Model  
339 Parameter Estimation Experiment).

340 This paper is structured as follows. In the Methods section, we describe two of our proposed modules, i.e.  
341 HSC and HSC-MCT, and two benchmark models (HBV, TOPMODEL). This section also includes the  
342 description of other modules (i.e. interception, evaporation and routing) in rainfall-runoff modelling, and  
343 the methods for model evaluation, calibration and validation. The Dataset section reviews the empirically-  
344 based knowledge of the Bruntland Burn catchment in Scotland and the hydrometeorological and  
345 topographic datasets of MOPEX catchments in the US for model comparison. The Results section presents  
346 the model comparison results. The Discussion section interprets the relation between rainfall-runoff  
347 processes and topography, catchment heterogeneity and simple model, and the implications and  
348 limitations of our proposed modules. The conclusions are briefly reviewed in the Summary and  
349 Conclusions section.

## 350 2 Methods

351 Based on our perceptual model that saturation excess flow (SEF) is the dominant runoff generation  
352 mechanism in most cases, we developed the HAND-based Storage Capacity curve (HSC) module.  
353 Subsequently, estimating the parameter of root zone storage capacity ( $S_{uMax}$ ) by the MCT method without  
354 calibration, the HSC-MCT was developed. In order to assess the performance of our proposed modules,  
355 two widely-used runoff generation modules, i.e. HBV power function and TOPMODEL module, were set  
356 as benchmarks. Other modules, i.e. interception, evaporation and routing, are kept with identical  
357 structure and parameterization for the four rainfall-runoff models (HBV, TOPMODEL, HSC, HSC-MCT,  
358 whose names are from their runoff generation modules), to independently diagnose the difference among  
359 runoff generation modules ([Clark et al., 2008; 2010](#)).

### 360 2.1 Two benchmark modules

#### 361 **HBV power function**

362 The HBV runoff generation module applies an empirical power function to estimate the nonlinear  
 363 relationship between the runoff coefficient and soil moisture ([Bergström and Forsman, 1973; Bergström](#)  
 364 [and Lindström, 2015](#)). The function is written as:

$$365 \quad A_s = \left( \frac{S_u}{S_{uMax}} \right)^\beta \quad (1)$$

366 Where  $A_s$  (-) represents the contributing area, which equals to the runoff coefficient of a certain rainfall  
 367 event;  $S_u$  (mm) represents the averaged root zone soil moisture;  $S_{uMax}$  (mm) is the averaged root zone  
 368 storage capacity of the studied catchment;  $\beta$  (-) is the parameter determining the shape of the power  
 369 function. The prior range of  $\beta$  can be from 0.1 to 5. The  $S_u$  -  $A_s$  has a linear relation while  $\beta$  equals to 1. And  
 370 the shape becomes convex while the  $\beta$  is less than 1, and the shape turns to concave while the  $\beta$  is larger  
 371 than 1. In most situations,  $S_{uMax}$  and  $\beta$  are two free parameters, cannot be directly measured at the  
 372 catchment scale, and need to be calibrated based on observed rainfall-runoff data.

373 **TOPMODEL module**

374 The TOPMODEL assumes topographic information captures the runoff generation heterogeneity at  
 375 catchment scale, and the TWI is used as an index to identify rainfall-runoff similarity ([Beven and Kirkby,](#)  
 376 [1979; Sivapalan et al., 1997](#)). Areas with similar TWI values are regarded as possessing equal runoff  
 377 generation potential. More specifically, the areas with larger TWI values tend to be saturated first and  
 378 contribute to SEF; but the areas with lower TWI values need more water to reach saturation and generate  
 379 runoff. The equations are written as follow:

$$380 \quad D_i = \bar{D} + S_{uMax} (\bar{I}_{TW} - I_{TW_i}) \quad (2)$$

$$381 \quad \bar{D} = S_{uMax} - S_u \quad (3)$$

$$382 \quad A_s = \sum A_{s_i}; \quad \text{while } D_i < 0 \quad (4)$$

383 Where  $D_i$  (mm) is the local storage deficit below saturation at specific location ( $i$ );  $\bar{D}$  (mm) is the averaged  
 384 water deficit of the entire catchment (Equation 2), which equals to  $(S_{uMax} - S_u)$ , as shown in Equation 3.  $I_{TW_i}$   
 385 is the local  $I_{TW}$  value.  $\bar{I}_{TW}$  is the averaged TWI of the entire catchment. Equation 2 means in a certain soil  
 386 moisture deficit condition for the entire catchment ( $\bar{D}$ ), the soil moisture deficit of a specific location ( $D_i$ ),  
 387 is determined by the catchment topography ( $I_{TW}$  and  $I_{TW_i}$ ), and the root zone storage capacity ( $S_{uMax}$ ).

388 Therefore, the areas with  $D_i$  less than zero are the saturated areas ( $A_{s\_i}$ ), equal to the contributing areas.  
389 The integration of the  $A_{s\_i}$  areas ( $A_s$ ), as presented in Equation 4, is the runoff contributing area, which  
390 equals to the runoff coefficient of that rainfall event.

391 Besides continuous rainfall-runoff calculation, Equations 2-4 also allow us to obtain the contributing area  
392 ( $A_s$ ) from the estimated relative soil moisture ( $S_u/S_{u\text{Max}}$ ), and then map it back to the original TWI map,  
393 which makes it possible to test the simulated contributing area by field measurement. It is worth  
394 mentioning that the TOPMODEL in this study is a simplified version, and not identical to the original one,  
395 which combines the saturated and unsaturated soil components.

## 396 2.2 HSC module

397 In the HSC module, we assume 1) SEF is the dominant runoff generation mechanism, while surface  
398 overland flow (SOF) and subsurface flow (SSF) cannot be distinguished; 2) the local root zone storage  
399 capacity has a positive and linear relationship with HAND, from which we can derive the spatial  
400 distribution of the root zone storage capacity; 3) rainfall firstly feeds local soil moisture deficit, and no  
401 runoff can be generated before local soil moisture being saturated.

402 Figure 24 shows the perceptual HSC module, in which we simplified the complicated 3-D topography of a  
403 real catchment into a 2-D simplified hillslope. And then derive the distribution of root zone storage  
404 capacity, based on topographic analysis and the second assumption as mentioned in the preceding  
405 paragraph. Figure 32 shows the approach to derive the  $S_u$ - $A_s$  relation, which are detailed as follows.

- 406 I. **Generate HAND map.** The HAND map, which represents the relative vertical distance to the  
407 nearest river channel, can be generated from DEM (Gharari et al., 2011). The stream initiation  
408 threshold area is a crucial parameter, determining the perennial river channel network  
409 (Montgomery and Dietrich, 1989; Hooshyar et al., 2016), and significantly impacting the HAND  
410 values. In this study, the start area was chosen as 40ha for the BB catchment to maintain a close  
411 correspondence with observed stream network. And for the MOPEX catchments, the stream  
412 initiation area threshold is set as 500 grid cells ( $4.05 \text{ km}^2$ ), which fills in the range of stream  
413 initiation thresholds reported by others (e.g. Colombo et al., 2007; Moussa, 2008, 2009). HAND  
414 maps were then calculated from the elevation of each raster cell above nearest grid cell flagged  
415 as stream cell following the flow direction (Gharari et al., 2011).
- 416 II. **Generate normalized HAND distribution curve.** Firstly, sort the HAND values of grid cells in  
417 ascending order. Secondly, the sorted HAND values were evenly divided into  $n$  bands (e.g. 20

bands in this study), to make sure each HAND band has similar area. The averaged HAND value of each band is regarded as the HAND value of that band. Thirdly, normalize the HAND bands, and then plot the normalized HAND distribution curve (Figure 24b).

III. **Distribute  $S_{u\text{Max}}$  to each HAND band ( $S_{u\text{Max}_i}$ )**. As assumed, the normalized storage capacity of each HAND band ( $S_{u\text{Max}_i}$ ) increases with HAND value (Figure 24c). Based on this assumption, the unsaturated root zone storage capacity ( $S_{u\text{Max}}$ ) can be distributed to each HAND band as  $S_{u\text{Max}_i}$  (Figure 32a). It is worth noting that  $S_{u\text{Max}}$  needs to be calibrated in the HSC module, but free of calibration in the HSC-MCT module.

IV. **Derive the  $S_u$  -  $A_s$  curve**. With the number of  $s$  saturated HAND bands (Figure 32a-c), the soil moisture ( $S_u$ ) can be obtained by Equation 5; and saturated area proportion ( $A_s$ ) can be obtained by Equation 6.

$$S_u = \frac{1}{n} [\sum_{i=1}^s S_{u\text{Max}_i} + S_{u\text{Max}_s} (n - s)] \quad (5)$$

$$A_s = \frac{s}{n} \quad (6)$$

Where  $S_{u\text{Max}_s}$  is the maximum  $S_{u\text{Max}_i}$  of all the saturated HAND bands. Subsequently, the  $A_s$  -  $S_u$  curve can be derived, and shown in Figure 32d.

The SEF mechanism assumes that runoff is only generated from saturation areas, therefore the proportion of saturation area is equal to the runoff coefficient of that rainfall-runoff event. Based on the  $S_u$ - $A_s$  curve in Figure 2d3d, generated runoff can be calculated from root zone moisture ( $S_u$ ). The HSC module also allows us to map out the fluctuation of saturated areas by the simulated catchment average soil moisture. For each time step, the module can generate the simulated root zone moisture for the entire basin ( $S_u$ ). Based on the  $S_u$ - $A_s$  relationship (Figure 2d3d), we can map  $S_u$  back to the saturated area proportion ( $A_s$ ) and then visualize it in the original HAND map. Based on this conceptual model, we developed the computer program and created a procedural module. The technical roadmap can be found in Figure 34.

### 2.3 HSC-MCT module

The  $S_{u\text{Max}}$  is an essential parameter in various hydrological models (e.g. HBV, Xinanjiang, GR4J), which determines the long-term partitioning of rainfall into infiltration and runoff. Gao et al., 2014a found that  $S_{u\text{Max}}$  represents the adaption of ecosystems to local climate. Ecosystems may design their  $S_{u\text{Max}}$  based on the precipitation pattern and their water demand. The storage is neither too small to be mortal in dry seasons, nor too large to consume excessive energy and nutrients. Based on this assumption, we can estimate the  $S_{u\text{Max}}$  without calibration, by the MCT method, from climatological and vegetation

448 information. More specifically, the average annual plant water demand in the dry season ( $S_R$ ) is  
449 determined by the water balance and the vegetation phenology, i.e. precipitation, runoff and seasonal  
450 NDVI. Subsequently, based on the annual  $S_R$ , the Gumbel distribution ([Gumbel, 1935](#)), frequently used for  
451 estimating hydrological extremes, was used to standardize the frequency of drought occurrence.  $S_{R20y}$ , i.e.  
452 the root zone storage capacity required to overcome a drought once in 20 years, is used as the proxy for  
453  $S_{uMax}$  due to the assumption of a “cost” minimization strategy of plants as we mentioned above ([Milly, 1994](#)), and the fact that  $S_{R20y}$  has the best fit with  $S_{uMax}$ . The  $S_{R20y}$  of the MOPEX catchments can be found  
454 in the map of ([Gao et al., 2014a](#)).

455  
456 Eventually, with the MCT approach to estimate  $S_{uMax}$  and the HSC curve to represent the root zone storage  
457 capacity spatial distribution, the HSC-MCT runoff generation module is created, without free parameters.  
458 It is worth noting that both the HSC-MCT and HSC modules are based on the HAND derived  $S_u$ - $A_s$  relation,  
459 and their distinction lays in the methods to obtain  $S_{uMax}$ . So far, the HBV power function module has 2 free  
460 parameters ( $S_{uMax}$ ,  $\beta$ ). While the TOPMODEL and the HSC both have one free parameter ( $S_{uMax}$ ). Ultimately  
461 the HSC-MCT has no free parameter.

## 462 2.4 Interception, evaporation and routing modules

463 Except for the runoff generation module in the root zone reservoir ( $S_{UR}$ ), we need to consider other  
464 processes, including interception ( $S_{IR}$ ) before the  $S_{UR}$  module, evaporation from the  $S_{UR}$  and the response  
465 routine ( $S_{FR}$  and  $S_{SR}$ ) after runoff generation from  $S_{UR}$  ([Figure 45](#)). Precipitation is firstly intercepted by  
466 vegetation canopies. In this study, the interception was estimated by a threshold parameter ( $S_{iMax}$ ), set to  
467 2 mm ([Gao et al., 2014a](#)), below which all precipitation will be intercepted and evaporated (Equation 9)  
468 ([de Groen and Savenije, 2006](#)). For the  $S_{UR}$  reservoir, we can either use the HBV beta-function (Equation  
469 12), the runoff generation module of TOPMODEL (Equation 2-4) or the HSC module (Section 2.3) to  
470 partition precipitation into generated runoff ( $R_u$ ) and infiltration. The actual evaporation ( $E_a$ ) from the soil  
471 equals to the potential evaporation ( $E_p$ ), if  $S_u/S_{uMax}$  is above a threshold ( $C_e$ ), where  $S_u$  is the soil moisture  
472 and  $S_{uMax}$  is the catchment averaged storage capacity. And  $E_a$  linearly reduces with  $S_u/S_{uMax}$ , while  $S_u/S_{uMax}$   
473 is below  $C_e$  (Equation 13). The  $E_p$  can be calculated by the Hargreaves equation (Hargreaves and Samani,  
474 1985), with maximum and minimum daily temperature as input. The generated runoff ( $R_u$ ) is further split  
475 into two fluxes, including the flux to the fast response reservoir ( $R_f$ ) and the flux to the slow response  
476 reservoir ( $R_s$ ), by a splitter ( $D$ ) (Equation 14, 15). The delayed time from rainfall peak to the flood peak is  
477 estimated by a convolution delay function, with a delay time of  $T_{lagF}$ . Subsequently, the fluxes into two  
478 different response reservoirs ( $S_{FR}$  and  $S_{SR}$ ) were released by two linear equations between discharge and

479 storage (Equation 19, 21), representing the fast response flow and the slow response flow mainly from  
480 groundwater reservoir. The two discharges ( $Q_f$  and  $Q_s$ ) generated the simulated streamflow ( $Q_m$ ). The  
481 model parameters are shown in Table 1, while the equations are given in Table 2. More detailed  
482 description of the model structure can be referred to [Gao et al., 2014b and 2016](#). It is worth underlining  
483 that the only difference among the benchmark HBV type, TOPMODEL type, ~~the~~-HSC<sub>2</sub> and ~~the~~-HSC-MCT  
484 models is their runoff generation modules. Eventually, there are 7 free parameters in HBV model, 6 in  
485 TOPMODEL and HSC model, and 5 in the HSC-MCT model.

## 486 2.5 Model evaluation, calibration, validation and models comparison

487 Two objective functions were used to evaluate model performance, since multi-objective evaluation is a  
488 more robust approach to quantifying model performance with different criteria than a single one. The  
489 Kling-Gupta efficiency ([Gupta et al., 2009](#)) ( $I_{KGE}$ ) was used as the criteria to evaluate model performance  
490 and as an objective function for calibration. The equation is written as:

$$491 I_{KGE} = 1 - \sqrt{(r-1)^2 + (\alpha-1)^2 + (\varepsilon-1)^2} \quad (7)$$

492 Where  $r$  is the linear correlation coefficient between simulation and observation;  $\alpha$  ( $\alpha = \sigma_m / \sigma_o$ ) is a  
493 measure of relative variability in the simulated and observed values, where  $\sigma_m$  is the standard deviation  
494 of simulated streamflow, and  $\sigma_o$  is the standard deviation of observed streamflow;  $\varepsilon$  is the ratio between  
495 the average value of simulated and observed data. And the  $I_{KGL}$  ( $I_{KGE}$  of the logarithmic flows) ([Fenia et](#)  
496 [al., 2007; Gao et al., 2014b](#)) is used to evaluate the model performance on baseflow simulation.

497 A multi-objective parameter optimization algorithm (MOSCEM-UA) ([Vrugt et al., 2003](#)) was applied for  
498 the calibration. The parameter sets on the Pareto-frontier of the multi-objective optimization were  
499 assumed to be the behavioral parameter sets and can equally represent model performance. The  
500 averaged hydrograph obtained by all the behavioral parameter sets were regarded as the simulated result  
501 of that catchment for further studies. The number of complexes in MOSCEM-UA were set as the number  
502 of parameters (7 for HBV, 6 for TOPMODEL and the HSC model, and 5 for HSC-MCT model), and the  
503 number of initial samples was set to 210 and a total number of 50000 model iterations for all the  
504 catchment runs. For each catchment, the first half period of data was used for calibration, and the other  
505 half was used to do validation.

506 In module comparison, we defined three categories: if the difference of  $I_{KGE}$  of model A and model B in  
507 validation is less than 0.1, model A and B are regarded as “equally well”. If the  $I_{KGE}$  of model A is larger

508 than model B in validation by 0.1 or more, model A is regarded as outperforming model B. If the  $I_{KGE}$  of  
509 model A is less than model B in validation by -0.1 or less, model B is regarded ~~to-as~~ outperform~~ing~~ model  
510 A.

## 511 3 Dataset

### 512 3.1 The Bruntland Burn catchment

513 The 3.2 km<sup>2</sup> Bruntland Burn catchment (Figure 56), located in north-eastern Scotland, was used as a  
514 benchmark study to test the models performance based on a rich data base of hydrological measurements.  
515 The Bruntland Burn is a typical upland catchment in North West Europe (e.g. [Birkel et al., 2010](#)), namely  
516 a combination of steep and rolling hillslopes and over-widened valley bottoms due to the glacial legacy of  
517 this region. The valley bottom areas are covered by deep (in parts > 30m) glacial drift deposits (e.g. till)  
518 containing a large amount of stored water superimposed on a relatively impermeable granitic solid  
519 geology ([Soulsby et al., 2016](#)). Peat soils developed (> 1m deep) in these valley bottom areas, which  
520 remain saturated throughout most of the year with a dominant near-surface runoff generation  
521 mechanism delivering runoff quickly via micro-topographical flow pathways connected to the stream  
522 network ([Soulsby et al., 2015](#)). Brown rankers, peaty rankers and peat soils are responsible for a flashy  
523 hydrological regime driven by saturation excess overland flow, while humus iron podzols on the hillslopes  
524 do not favor near-surface saturation but rather facilitate groundwater recharge through vertical water  
525 movement ([Tetzlaff et al., 2014](#)). Land-use is dominated by heather moorland, with smaller areas of rough  
526 grazing and forestry on the lower hillslopes. Its annual precipitation is 1059 mm, with the summer months  
527 (May-August) generally being the driest ([Ali et al., 2013](#)). Snow makes up less than 10% of annual  
528 precipitation and melts rapidly below 500m. The evapotranspiration is around 400 mm per year and  
529 annual discharge around 659 mm. The daily precipitation, potential evaporation, and discharge ~~data~~ range  
530 from January 1 in 2008 to September 30 in 2014. The ~~data calibration period is~~ from January 1, 2008 to  
531 December 31, 2010~~is used as calibration~~, and the data from January 1, 2011 to September 30, 2014 is  
532 used as validation.

533 The LiDAR-derived DEM map with 2m resolution shows elevation ranging from 250m to 539m (Figure 56).  
534 There are 7 saturation area maps (Figure 67) (May 2, July 2, August 4, September 3, October 1, November  
535 26, in 2008, and January 21, in 2009), measured directly by [the](#) “squishy boot” method and field mapping  
536 by global positioning system (GPS), to delineate the boundary of saturation areas [connected to the stream](#)  
537 [network](#) ([Birkel et al., 2010](#); [Ali et al., 2013](#)). These saturation area maps revealed a dynamic behavior of

538 expanding and contracting areas connected to the stream network that were used as a benchmark test  
539 for the HSC module.

540 **3.2 MOPEX ~~dataset~~ catchments**

541 The MOPEX dataset was collected for a hydrological model parameter estimation experiment (Duan et al.,  
542 2006; Schaake et al., 2006), containing 438 catchments in the CONUS (Contiguous United States). The  
543 longest time series range from 1948 to 2003. 323 catchments were used in this study (see the name list  
544 in SI), with areas between 67 and 10,329 km<sup>2</sup>, and excluding the catchments with data records <30 years,  
545 impacted by snowmelt or with extreme arid climate (aridity index  $E_p/P > 2$ ). In order to analyze ~~see the~~  
546 impacts of catchment characteristics on model performance, except for excluding hydrometeorology data,  
547 we also collected the datasets of topography, depth to rock, soil texture, land use, and stream density  
548 (Table 3). These characteristics help us to understand in which catchments the HSC performs better or  
549 worse than the benchmark models.

550 **Hydrometeorology data**

551 ~~The MOPEX dataset was collected for a hydrological model parameter estimation experiment (Duan et al.,~~  
552 ~~2006; Schaake et al., 2006), containing 438 catchments in the CONUS (Contiguous United States). The~~  
553 dataset contains the daily precipitation, daily maximum and minimum air temperature, and daily  
554 streamflow. ~~The longest time series range from 1948 to 2003. 323 catchments were used in this study~~  
555 ~~(see the name list in SI), with areas between 67 and 10,329 km<sup>2</sup>, and excluding the catchments with data~~  
556 ~~records <30 years, impacted by snowmelt or with extreme arid climate (aridity index  $E_p/P > 2$ ). The daily~~  
557 streamflow was used to calibrate the free parameters, and validate the models.

558 **Topography data**

559 The Digital Elevation Model (DEM) of the CONUS in 90m resolution was download from the Earth Explorer  
560 of United States Geological Survey (USGS, <http://earthexplorer.usgs.gov/>). The HAND and TWI map can  
561 be generated from DEM. The averaged elevation and HAND are used to as two catchment characteristics.

562 **Soil texture**

563 Soil texture is complex. In this study, soil texture is synthetically represented by the K factor, since the K  
564 factor is a lumped soil erodibility factor which represents the soil profile reaction to soil detachment  
565 (Renard et al., 2011). Generally, the soils (high in clay and sand) have low K values, and soils with high silt

566 content have larger K values. The averaged K factor for each catchment was calculated from soil survey  
567 information available from USGS (Wolock, 1997).

568 **Land use**

569 Land use data was obtained from National Land Cover Database (NLCD, <http://www.mrlc.gov/nlcd.php>).  
570 Forest plays an essential role in hydrological processes (Gao et al., 2018a), especially for the runoff  
571 generation (Brooks et al., 2010). Forest area proportion was utilized as an integrated indicator to represent  
572 the impact of vegetation cover on hydrological processes.

573 **Stream density**

574 Stream density (km/km<sup>2</sup>) is the total length of all the streams and rivers in a drainage basin divided by the  
575 total area of the drainage basin. Stream density data was obtained from Horizon Systems Corporation  
576 (<http://www.horizon-systems.com/nhdplus/>).

577 **Geology**

578 Bedrock is a relative impermeable layer, as the lower boundary of subsurface stormflow in the catchments  
579 where soil depth is shallow (Tromp-van Meerveld & McDonnell). The depth to bedrock, as an integrated  
580 geologic indicator, was accessed from STATSGO (State Soil Geographic,  
581 [http://www.soilinfo.psu.edu/index.cgi?soil\\_data&conus&data\\_cov&dtb](http://www.soilinfo.psu.edu/index.cgi?soil_data&conus&data_cov&dtb) (Schwarz & Alexander, 1995).

582 The averaged depth to bedrock for each catchment was calculated for further analysisby using the and  
583 used for further analysis.

584 **4 Results of the Bruntland Burn**

585 **4.1 Topography analysis**

586 The generated HAND map, derived also from the DEM, is shown in Figure 56, with HAND values ranging  
587 from 0m to 234m. Based on the HAND map, we can derive the  $S_u$ - $A_s$  curve (Figure 78) by analyzing the  
588 HAND map with the method in Section 2.3. The TWI map of the BB (Figure 56) was generated from its  
589 DEM. Overall, the TWI map, ranging from -0.4 to 23.4, mainly differentiates the valley bottom areas with  
590 the highest TWI values from the steeper slopes. This is probably caused by the fine resolution of the DEM  
591 map in 2 m, since as previous research found that the sensitivity of TWI to DEM resolution (Sørensen and  
592 Seibert, 2007). From the TWI map, the frequency distribution function and the accumulative frequency  
593 distribution function can be derived (Figure 78), with one unit of TWI as interval.

594 4.2 Model performance

595 It is found that all the three models (HBV, TOPMODEL, and HSC) can perform well ~~in~~ reproducing the  
596 observed hydrograph (Figure 89). The  $I_{KGE}$  of the three models are all around 0.66 in calibration, which is  
597 largely in line with other studies from the BB (Birkel et al, 2010; 2014). And the  $I_{KGL}$  are 0.76, 0.72 and 0.74  
598 for HSC, HBV and TOPMODEL respectively in calibration. While in validation,  $I_{KGE}$  of ~~the~~ three models are  
599 also around 0.66, while  $I_{KGL}$  are 0.75, 0.70 and 0.65 for the three models. Since the measured rainfall-  
600 runoff time series only last~~s~~ from 2008 to 2014, which is too short to estimate the  $S_{R20y}$  (proxy for  $S_{uMax}$ )  
601 by MCT approach (which needs long-term hydro-meteorological observation data,) the HSC-MCT model  
602 was not applied to ~~the~~is catchment.

603 Figure 8 shows the calibrated power curve by HBV (averaged beta=0.98) with the  $S_u$ - $A_s$  curve obtained  
604 from the HSC module. We found the two curves are largely comparable, especially while the relative soil  
605 moisture is low. This result demonstrates that for the BB catchment with glacial drift deposits and  
606 combined terrain of steep and rolling hillslopes and over-widened valley bottoms, the HBV power curve  
607 can essentially be derived from the  $S_u$ - $A_s$  curve of HSC module merely by topographic information without  
608 calibration.

609 The normalized relative soil moisture of the three model simulations are presented in Figure 89. Their  
610 temporal fluctuation patterns are comparable. Nevertheless, the simulated soil moisture by TOPMODEL  
611 has a larger variation, compared with HBV and HSC (Figure 89).

612 ~~Figure 7 shows the calibrated power curve from HBV (averaged beta=0.98) with the  $S_u$ - $A_s$  curve obtained~~  
613 ~~from the HSC module. We found the two curves are largely comparable, especially while the relative soil~~  
614 ~~moisture is low. This result demonstrates that for the BB with glacial drift deposits and combined terrain~~  
615 ~~of steep and rolling hillslopes and over-widened valley bottoms, the HBV power curve can essentially be~~  
616 ~~derived from the  $S_u$ - $A_s$  curve of HSC module merely by topographic information without calibration.~~

617 4.3 Contributing area simulation

618 The observed saturation area and the simulated contributing area from both TOPMODEL and the HSC are  
619 shown in Figure 67, 98, 109. We found although both modules overestimated the ~~contributing saturated~~  
620 areas, they can capture the temporal variation. For example, the smallest saturated area both observed  
621 and simulated occurred on July-02-2008, and the largest saturated area both occurred on January-21-  
622 2009. Comparing the estimated contributing area of TOPMODEL with the HSC module, we found the  
623 results of the HSC correlates better ( $R^2=0.60$ ,  $I_{KGE}=-3.0$ ) with the observed saturated areas than TOPMODEL

624 ( $R^2=0.50$ ,  $I_{KGE}=-3.4$ ) (Figure 910). For spatial patterns, the HSC saturated contributing area simulated by  
625 HSC module is located near close to the river channel network, and reflects the spatial pattern of observed  
626 saturated area. But While TOPMODEL results are more scattered, probably due to the sensitivity of TWI to DEM resolution  
627 the results of the HSC module are also more closely comparable with the observed saturated areas than TOPMODEL (Figure 67). And the HSC is more discriminating in terms of  
628 less frequently giving an unrealistic 100% catchment saturation, and retaining parts of the unsaturated  
629 upper hillslopes. Based on these results benchmarking the HSC module with observed saturated area  
630 maps, we proceeded to test HSC for a wide range of climatically and geomorphologically different  
631 catchments across the US.

## 633 5 Results from the MOPEX catchments

### 634 5.1 Topography analysis of the Contiguous US and 323 MOPEX catchments

635 To delineate the TWI map for the CONUS, the depressions of the DEM were firstly filled with a threshold  
636 height of 100m (recommended by Esri). The TWI map of the CONUS is produced (Figure S1). Based on the  
637 TWI map of the CONUS, we clipped the TWI maps for the 323 MOPEX catchments with their catchment  
638 boundaries. And then the TWI frequency distribution and the accumulated frequency distribution of the  
639 323 MOPEX catchments (Figure S2), with one unit of TWI as interval, were derived based on the 323 TWI  
640 maps.

641 In Figure 1011, it is shown that the regions with large HAND values are located in Rocky Mountains and  
642 Appalachian Mountains, while the Great Plains has smaller HAND values. Interestingly, the Great Basin,  
643 especially in the Salt Lake Desert, has small HAND values, illustrating its low elevation above the nearest  
644 drainage, although their elevations above sea level are high. From the CONUS HAND map, we clipped the  
645 HAND maps for the 323 MOPEX catchments with their catchment boundaries. We then plot their HAND-  
646 area curves, following the procedures of I and II in Section 2.2. Figure 11a-12a shows the normalized HAND  
647 profiles of the 323 catchments.

648 Based on the HAND profiles and the Step III in Section 2.2, we derived the normalized storage capacity  
649 distribution for all catchments (Figure 11b-12b). Subsequently, the root zone moisture and saturated area  
650 relationship ( $A_s-S_u$ ) can be plotted by the method in Step IV of Section 2.2. Lastly, reversing the curve of  
651  $A_s-S_u$  to  $S_u-A_s$  relation (Figure 11c-12c), the latter one can be implemented to simulate runoff generation  
652 by soil moisture. Figure 11c-12c interestingly shows that in some catchments, there is almost no threshold  
653 behavior between rainfall and runoff generation, where the catchments are covered by large areas with

654 low HAND values and limited storage capacity. Therefore, when rainfall occurs, wetlands response quickly  
655 and generate runoff without a precipitation–discharge threshold relationship characteristic of areas with  
656 higher moisture deficits. This is similar to the idea of FLEX-Topo where the storage capacity is distinguished  
657 between wetlands and hillslopes, and on wetlands, with low storage capacity, where runoff response to  
658 rainfall is almost instantaneous.

659 **5.2 Model performance**

660 Overall, the performance of the two benchmark models, i.e. HBV and TOPMODEL, for the MOPEX data  
661 (Figure 1213) is comparable with the previous model comparison experiments, conducted with four  
662 rainfall-runoff models and four land surface parameterization schemes (Duan et al., 2006; Kollat et al.,  
663 2012; Ye et al., 2014). The median value of  $I_{KGE}$  of the HBV type model is 0.61 for calibration in the 323  
664 catchments (Figure 1213), and averaged  $I_{KGE}$  in calibration is 0.62. In validation, the median and averaged  
665 values of  $I_{KGE}$  are kept the same as calibration. The comparable performance of models in calibration and  
666 validation demonstrates the robustness of benchmark models and the parameter optimization algorithm  
667 (i.e. MOSCEM-UA). The TOPMODEL improves the median value of  $I_{KGE}$  from 0.61 (HBV) to 0.67 in  
668 calibration, and from 0.61 (HBV) to 0.67 in validation. But the averaged values of  $I_{KGE}$  for TOPMODEL are  
669 slightly decreased from 0.62 (HBV) to 0.61 in both calibration and validation. The HSC module, by involving  
670 the HAND topographic information without calibrating the  $\beta$  parameter, improves the median value of  
671  $I_{KGE}$  to 0.68 for calibration and 0.67 for validation. The averaged values of  $I_{KGE}$  in both calibration and  
672 validation are also increased to 0.65, comparing with HBV (0.62) and TOPMODEL (0.61). Furthermore,  
673 Figure 1213 demonstrates that, comparing with the benchmark HBV and TOPMODEL, not only the median  
674 and averaged values were improved by the HSC module, but also the 25<sup>th</sup> and 75<sup>th</sup> percentiles and the  
675 lower whisker end, all have been improved. The performance gains on baseflow ( $I_{KGL}$ ) have been  
676 investigated and shown in the supplementary figure S3. These results indicate the HSC module improved  
677 model performance to reproduce hydrograph for both peak flow ( $I_{KGE}$ ) and baseflow ( $I_{KGL}$ ).

678 Additionally, for HSC-MCT model, the median  $I_{KGE}$  value is improved from 0.61 (HBV) to 0.65 in calibration,  
679 and from 0.61 (HBV) to 0.64 in validation, but not as well performed as TOPMODEL (0.67 for calibration  
680 and validation). For the averaged  $I_{KGE}$  values, they were slightly reduced from 0.62 (HBV) and 0.61  
681 (TOPMODEL) to 0.59 for calibration and validation. Although the HSC-MCT did not perform as well as the  
682 HSC module, considering there is no free parameters to calibrate, the median  $I_{KGE}$  value of 0.64 (HBV is  
683 0.61) and averaged  $I_{KGE}$  of 0.59 (TOPMODEL is 0.61) are quite acceptable. In addition, the 25<sup>th</sup> and 75<sup>th</sup>  
684 percentiles and the lower whisker end of the HSC-MCT model are all improved compared to the HBV

685 model. Moreover, the largely comparable results between the HSC and the HSC-MCT modules  
686 demonstrate the feasibility of the MCT method to obtain the  $S_{u\text{Max}}$  parameter and the potential for HSC-  
687 MCT to be implemented in prediction of ungauged basins.

688 Figure 13-14 shows the spatial comparisons of the HSC and HSC-MCT models with the two benchmark  
689 models. We found that the HSC performs “equally well” as HBV (the difference of  $I_{KGE}$  in validation ranges  
690  $-0.1 \sim 0.1$ ) in 88% catchments, and in the remaining 12% of the catchments the HSC outperforms HBV (the  
691 improvement of  $I_{KGE}$  in validation is larger than 0.1). In not a single catchment did the calibrated HBV  
692 outperform the HSC. Comparing the HSC model with TOPMODEL, we found in 91% of the catchments that  
693 the two models have approximately equal performance. In 8% of the catchments, the HSC model  
694 outperformed TOPMODEL. Only in 1% of the catchments (two in the Appalachian Mountains and one in  
695 the Rocky Mountains in California), TOPMODEL performed better.

696 In order to further explore the impact of catchment characteristics on model performance, we used  
697 topography (averaged HAND, averaged slope, and averaged elevation), soil (K-factor), land cover (forest  
698 area proportion), climate (aridity index), stream density, and geology (depth to rock) information to  
699 testsee the impact of catchment features on model performance. Table 4 clearly shows that compared  
700 with HBV, the 39 catchments with better performance have loweress HAND values (37m), more gentle  
701 slopes (4.0 degree), and smaller forest area (22%); while the elevation, K-factor, aridity index, stream  
702 density and depth to rock are almost similar. Also, in the catchments where HSC outperformed  
703 TOPMODEL, the catchments have smaller HAND (27m), more gentle slopes (3.6 degree), moderate  
704 elevation (469 m), less forest proportion (14%), and more arid climatearea (aridity index is 1.3).  
705 TOPMODEL performs better in only three catchments with larger HAND (193m), steeper slopes (13.5  
706 degree), higher elevation (740 m), more humid climate (aridity index is 0.8), and larger depth to rock (333  
707 cm). In summary,Summarily, the HSC showedhas better performance in-the catchments with gentle  
708 topography and more arid climate.

709 From the spatial comparison, we found that the catchments, where the HSC model performed better are  
710 mostly located in the Great Plains, with modest sloping (4.0 degree), while the other catchments have  
711 average slope of 8.1 degree. Comparing the HSC model with TOPMODEL, we found in 91% of the  
712 catchments that the two models have approximately equal performance. In 8% of the catchments, the  
713 HSC model outperformed TOPMODEL. Only in 1% of the catchments (two in Appalachian Mountain and  
714 one in the Rocky Mountain in California), TOPMODEL performed better. From spatial analysis, we found  
715 the HSC outperformed catchments have flat terrain (2.3 degree) with moderate averaged HAND value

716 (26m), while the TOPMODEL outperformed catchments have steep hillslope (19 degree) with large  
717 averaged HANd value (154m).

718 Without calibration of  $S_{u\text{Max}}$ , as expected, the performance of HSC-MCT module slightly deteriorates  
719 (Figure 1213). In comparison with HBV, the outperform~~ed percentage ance~~ reduced from 12% (HSC) to 4%  
720 (HSC-MCT), the approximately equal-well simulated catchments dropped from 88% to 79%, and the  
721 inferior performance increased from 0% to 17%. Also, in comparison with TOPMODEL, the better  
722 performance dropped from 8% (HSC~~model~~) to 7% (HSC-MCT~~model~~), the approximately equal catchments  
723 reduced from 91% to 72%, and the inferior performance increased from 1% to 21%. The inferiority of the  
724 HSC-MCT model is probably caused by the uncertainty of the MCT method for different ecosystems which  
725 have different survival strategies and use different return periods to bridge critical drought periods. By  
726 using ecosystem dependent return periods, this problem could be reduced (Wang-Erlundsson et al., 2016).

727

728 To further explore the reason for the better performance of the HSC approach, we selected the 08171000  
729 catchment in Texas (Figure 1314), in which both the HSC module and the HSC-MCT module outperformed  
730 the two benchmark modules to reproduce the observed hydrograph (Figure S4). The HBV model  
731 dramatically underestimated the peak flows, with  $I_{KGE}$  as 0.54, while TOPMODEL significantly  
732 overestimated the peak flows, with  $I_{KGE}$  as 0.30. The HSC-MCT model improved the  $I_{KGE}$  to 0.71, and the  
733 HSC model further enhanced  $I_{KGE}$  to 0.74.

734 Since the modules of interception, evaporation and routing are identical for the four models, the runoff  
735 generation modules are the key to understand the difference in model performance. Figure S5 shows the  
736 HBV  $\beta$  curve and the  $S_u$ - $A_s$  curve of the HSC model, as well the TWI frequency distribution. We found that  
737 with a given  $S_u/S_{u\text{Max}}$ , the HBV  $\beta$  function generates less contributing area than the HSC model, which  
738 explains the underestimation of the HBV model. In contrast, TOPMODEL has a sharp and steep  
739 accumulated TWI frequency curve. In particular, the region with TWI=8 accounts for 40% of the catchment  
740 area, and over 95% of the catchment areas are within the TWI ranging from 6 to 12. This indicates that  
741 even with low soil moisture content ( $S_u/S_{u\text{Max}}$ ), the contributing area by TOPMODEL is relatively large,  
742 leading to the sharply increased peak flows for all rainfall events.

743 6 Discussion

744 6.1 Rainfall-runoff processes and topography

745 We applied a novel approach to derive the relationship between soil moisture storage and the saturated  
746 area from HAND. The areas with relatively low HAND values are saturated earlier than areas with higher  
747 HAND values, due to the larger storage capacity in high~~er~~ HAND locations. The outperformance of the HSC  
748 ~~model~~ over the benchmark HBV and TOPMODEL in modestly-gentle sloping catchments indicates that that  
749 the HSC module likely has a higher realism than the calibrated HBV beta-function ~~of the HBV model~~ and  
750 the TWI of TOPMODEL in these regions. Very interestingly, [Fan et al., \(2017\)](#) presented an ecological  
751 observation in global ~~synthesis of 2,200 root observations of >1000 species scale~~, and revealed the  
752 systematic variation of rooting depth along HAND (Fig.1, in [Fan et al., 2017](#)). Since rooting depth can be  
753 translated to root zone storage capacity through combination with soil plant-available water ([Wang-](#)  
754 [Erlandsson et al., 2016](#)). This large sample dataset, from ecological perspective, provides a strong support  
755 for the assumption of the HSC model on modest-gentle slopes, i.e. the increase of root zone storage  
756 capacity with HAND. More interestingly, on excessively drained uplands, rooting depth does not follow  
757 the same pattern, with shallow depth and limited to rain infiltration (Fig.1, in [Fan et al., 2017](#)). This could  
758 explain the inferior performance of HSC model to TOPMODEL in three MOPEX catchments ~~(averaged~~  
759 ~~HAND is 154 m)~~ with excessively drained uplands (larger HAND, steeper slope, higher elevation, and  
760 deeper depth to rock), where Hortonian overland flow is likely the dominant mechanism, and the HSC  
761 assumption likely does not work well. This likely indicates that comparing with TWI, the HAND is closer to  
762 catchment realism to distinguishing hydrological similarity in gentle topography catchments.

763

764 The FLEX-Topo model ([Savenije, 2010](#)) also uses HAND ~~information~~ as a topographic index to distinguish  
765 between landscape-related runoff processes, and has both similarity and differences with the HSC model.  
766 The results of the HSC model illustrate that the riparian areas are more prone to be saturated, which is  
767 consistent with the concept of the FLEX-Topo model. Another important similarity of the two models is  
768 their parallel model structure. In both models it is assumed that the upslope area has larger storage  
769 capacity, therefore the upper land generates runoff less and later than the lower land. In other words, in  
770 most cases, the local storage is saturated due to the local rainfall, instead of flow from upslope. The most  
771 obvious difference between the HSC and the FLEX-Topo is the approach towards discretization of a  
772 catchment. The FLEX-Topo model classifies a catchment into various landscapes, e.g. wetlands, hillslopes

773 and plateau. This discretization method requires threshold values to classify landscapes, i.e. threshold  
774 values of HAN and slope, which leads to fixed and time-independent proportions of landscapes. The HSC  
775 model does not require landscape classification, which reduced the subjectivity in discretization and  
776 restricted the model complexity, as well as simultaneously allowing the fluctuation of ~~saturated~~  
777 ~~contributing~~ areas (termed as wetlands in FLEX-Topo).

778 ~~Except for topography, it is also interesting to test the impact of climate, geological, vegetation, and flow~~  
779 ~~characteristics on model efficiency. Gao et al., (2018) have conducted a study with the MOPEX dataset to~~  
780 ~~test the impact of various catchment characteristics on the shape of the beta function, and found that the~~  
781 ~~topographic information has the most significant impact on the shape of beta function. Therefore, we~~  
782 ~~merely investigated the impact of topography on beta function and model efficiency in this study.~~

## 783 6.2 Catchment heterogeneity and simple models

784 Catchments exhibit a wide array of heterogeneity and complexity with spatial and temporal variations of  
785 landscape characteristics and climate inputs. For example, the Darcy-Richards equation approach is often  
786 consistent with point-scale measurements of matrix flow, but not for preferential flow caused by roots,  
787 soil fauna and even cracks and fissures (Beven and Germann, 1982; Zehe and Fluehler, 2001; Weiler and  
788 McDonnell, 2007). As a result, field experimentalists continue to characterize and catalogue a variety of  
789 runoff processes, and hydrological and land surface modelers are developing more and more complicated  
790 models to involve the increasingly detailed processes (McDonnell et al., 2007). However, there is still no  
791 compelling evidence to support the outperformance of sophisticated “physically-based” models in terms  
792 of higher equifinality and uncertainty than the simple lumped or semi-distributed conceptual models in  
793 rainfall-runoff simulation (Beven, 1989; Orth et al., 2015).

794

795 But evidence is mounting that a catchment is not a random assemblage of different heterogeneous parts  
796 (Sivapalan, 2009; Troch et al., 2013; Zehe et al., 2013), and conceptualising heterogeneities does not  
797 require complex laws (Chase, 1992; Passalacqua et al., 2015). ~~P. Very parsimonious models (e.g. Perrin et~~  
798 ~~al., 2003), with empirical curve shapes, likely results in good model performance., the reduction of Hess~~  
799 ~~running space for Parameter identifiability in calibration is probably one of the reasons admittedly.~~  
800 ~~However, But the physical rationale of these parsimonious models it is still largely unknownn about the~~  
801 ~~reason rational of good performance these parsimonious models, and lacking aef the physically~~

802 explanation to interpret these empirical curves described by mathematical functions (e.g.  
803 Equation XX3 in Perrin et al., 2003).

804 The benefits of the new HSC module are two-fold. From a technical point of view, the HSC allows us to  
805 make Prediction in Ungauged Basins without calibrating the beta parameter in many conceptual  
806 hydrological models. Furthermore, the HSC module, from a scientific point of view, provides us with a new  
807 perspective on the linkage between the spatial distribution patterns of root zone storage capacity (long-  
808 term ecosystem evolution) with associated runoff generation (event scale rainfall-runoff generation). the  
809 ~~edsthe the -a Andwith sat with associated~~

810 Asking questions of “why” rather than “what” likely leads to more useful insights and a new way forward  
811 (McDonnell et al., 2007). The HSC module provides us with an explanationrationale from an ecological  
812 perspective to understand the linkage and mechanism between large-sample hillslope ecological observations  
813 and the curve of root zone storage capacity distribution (Figure 1, 2, 3). Catchment is a geomorphological and  
814 even an ecological system whose parts are related to each other probably due to catchment self-  
815 organization and evolution (Sivapalan and Blöschl, 2015; Savenije and Hrachowitz, 2017). This encourages  
816 the hope that simplified concepts may be found adequate to describe and model the operation of the  
817 basin runoff generation process. It is clear that topography, with fractal characteristic (Rodriguez-Iturbe  
818 and Rinaldo, 1997), is often the dominant driver of runoff, as well as being a good integrated indicator for  
819 vegetation cover (Gao et al., 2014b), rooting depth (Fan et al., 2017), root zone evaporation and  
820 transpiration deficits (Maxwell and Condon, 2016), soil properties (Seibert et al., 2007), and even geology  
821 (Rempe and Dietrich, 2014; Gomes, 2016). Therefore, we argue that increasingly detailed topographic  
822 information is an excellent integrated indicator allowing modelers to continue systematically represent  
823 heterogeneities and simultaneously reduce model complexity. The model structure and parameterization  
824 of both HSC and TOPMODEL are simple, but not over simplified, as they capture ~~probably likely~~ the most  
825 dominant factor controlling runoff generation, i.e. the spatial heterogeneity of storage capacity. Hence,  
826 this study also sheds light on the possibility of moving beyond heterogeneity and process complexity  
827 (McDonnell et al., 2007), to simplify them into a succinct and *a priori* curve by taking advantage of  
828 catchment self-organization probably caused by co-evolution or the principle of maximum entropy  
829 production (Kleidon and Lorenz, 2004).

### 830 6.3 Implications and limitation

831 The calibration-free HSC-MCT runoff generation ~~model module may~~ enhances our ability to predict runoff  
832 in ungauged basins. ~~Hydrological models still depend largely on observational data to feed statistical~~

833 ~~analysis and calibrate the free parameters. This~~PUB is probably not a major issue in the developed world,  
834 with abundant of comprehensive measurements in many places, but for the developing world it requires  
835 prediction with sparse data and fragmentary knowledge. Topographic information with high spatial  
836 resolution is freely available globally, allowing us to implement the HSC model in global scale studies. In  
837 addition, thanks to the recent development, testing, and validation of remote sensing evaporation  
838 products in large spatial scale (e.g. [Anderson et al., 2011](#); [Hu and Jia, 2015](#)), the  $S_{u\text{Max}}$  estimation has  
839 become possible without in situ hydro-meteorological measurements ([Wang-Erlansson et al., 2016](#)).  
840 These widely-accessible datasets make the global-scale implementation of HSC-MCT module promising.

841 Although the new modules perform well in the BB and the MOPEX catchments, we do not intend to  
842 propose “a model fits all”. ~~It is valuable to further test, to what extent the new concept (HAND is~~  
843 ~~proportional to storage capacity) reflects different geomorphological and geological processes. Also~~~~T~~he  
844 assumption of HSC, to some extent, is supported by large-sample ecological field observation ([Fan et al.,](#)  
845 [2017](#)), but it never means the  $A_s$ - $S_u$  curve of HSC can perfectly fit the other existing ~~modules~~curves (e.g.  
846 HBV and TOPMODEL). Unify all model approaches into one framework is the objective of several pioneer  
847 works (e.g. [Clark, et al., 2010](#); [Fenia et al., 2011](#)), but out of the scope of this study. Moreover, while  
848 estimating the runoff coefficient by the  $A_s$ - $S_u$  relation, rainfall in the early time may cause the increase of  
849  $S_u$ / $S_{u\text{Max}}$  and runoff coefficient ([Moore, 1985](#); [Wang, 2018](#)). Therefore neglecting this influence factor, HBV  
850 ~~module~~—(Equation 1), TOPMODEL (Equation 2-4) and HSC ~~module~~—(Equation 5-6) theoretically  
851 underestimate the runoff coefficient, which needs to be further investigated.

852 Finally, we should not ignore the limitations of the new module, although it has better performance and  
853 modelling consistency. 1) The threshold area for the initiating a stream was set as a constant value for the  
854 entire CONUS, but the variation of this value in different climate, geology and landscape classes  
855 ([Montgomery and Dietrich, 1989](#); [Helmlinger et al., 1993](#); [Colombo et al., 2007](#); [Moussa, 2008](#)) needs to be  
856 future investigated. 2) The discrepancy between observed and simulated saturation area needs to be  
857 further investigated, by utilizing more advanced field measurement and simultaneously refining the  
858 model assumption. To our understanding, there are two interpretations. Firstly, the overestimation of the  
859 HSC model is possibly because two runoff generation mechanisms – SOF and the SSF occur at the same  
860 time. However, the saturated area observed by the “squishy boot” method ([Ali et al., 2013](#)), probably only  
861 distinguished the areas where SOF occurred. Subsurface stormflow<sub>72</sub> also contribut~~ing~~es to runoff~~but~~  
862 ~~without surface runoff~~, cannot be observed by the “squishy boot” method. Thus, this mismatch between  
863 simulation and observation probably leads to this saturated area overestimation. The second

interpretation might be the different definition of "saturation". The observed saturated areas are places where 100% of soil pore volume is filled by water. But the modelled saturation areas are located where soil moisture is above field capacity, and not necessarily 100% filled with water, which probably also results in the overestimation of saturated areas. Interestingly, in theory the observed saturated area should be within the simulated contributing area, due to the fact that the saturated soil moisture is always larger than field capacity. From this point of view, the observed saturated area is smaller and within the contributing area boundary simulated by HSC, but TOPMODEL missed this important feature.<sup>3)</sup> <sup>4)</sup> Only the runoff generation module is calibration free, but the interception and response routines are still relied on calibration. Although we kept the interception and response routine modules the same for the four models, the variation of other calibrated parameters (i.e.  $S_{i\text{Max}}$ ,  $D$ ,  $K_f$ ,  $K_s$ ,  $T_{\text{lagF}}$ ) may also influence model performance in both calibration and validation. <sup>45)</sup> The computational cost of the HSC and MCT is much more expensive than the HBV, and similar to as TOPMODEL, due to the cost of preprocessed topographic analysis~~two benchmark models, especially comparing with HBV, because of the calculation of  $S_{i\text{Max}}$  by the MCT method, and the topographic analysis of the HSC module. But once the  $S_u$ - $A_s$  curve is completed, the computation cost is quite comparable with HBV.~~

## 7 Summary and conclusions

In this study, we developed a simple and calibration-free hydrological module (HAND-based Storage Capacity curve, HSC) based on a relative new topographic index (HAND), which is not only an excellent physically-based indicator ~~of for the hydrologic similarity and a physically-based index linking terrain with hydraulic gradient at the hillslope and catchment scales, but also represents the spatial distribution pattern of root zone storage capacity supported by large-sample ecological observations. We assumed that the local storage capacity is closely linked to HAND.~~ Based on ~~this assumption and the~~ HAND spatial distribution pattern, the soil moisture ( $S_u$ ) - saturated area ( $A_s$ ) relation for each catchment was derived, which was used to estimate the  $A_s$  of specific rainfall event based on continuous calculation of  $S_u$ . Subsequently, based on the  $S_u$ - $A_s$  relation, the HAND-based Storage Capacity curve (HSC) module was developed. Then, applying the mass curve technique (MCT) approach, we estimated the root zone storage capacity ( $S_{u\text{Max}}$ ) from observable hydro-climatological and vegetation data, and coupled it with HSC to create the calibration-free HSC-MCT module, ~~in which the  $S_{u\text{Max}}$  was obtained by MCT, and the  $S_u$ - $A_s$  relation was obtained by HSC. The HBV beta-function and TWI-based TOPMODEL were used as two~~ benchmarks to test the performance of HSC and HSC-MCT on both hydrograph simulation and ability to reproduce the contributing area, which was measured for different hydrometeorological conditions in the

895 Bruntland Burn catchment in Scotland. Subsequently, 323 MOPEX catchments in the US were used as a  
896 large-sample hydrological study to further validate the effectiveness of our proposed runoff generation  
897 modules.

898 In the BB exploratory study, we found that the HSC, HBV and TOPMODEL performed comparably well to  
899 reproduce the observed hydrograph. ~~Interestingly, the  $S_u$ - $A_u$  curves of HSC and HBV are largely comparable, which illustrates the HSC curve can likely be used as a proxy for the HBV beta-function.~~ Comparing the  
900 estimated contributing area of TOPMODEL with the HSC module, we found that ~~the results of the~~ HSC  
901 module ~~performed~~s better to reproduce saturated area variation, in terms of the correlation coefficient  
902 ~~correlate and spatial patterns~~, better ( $R^2=0.60$ ) with the observed saturated areas compared to  
903 TOPMODEL ( $R^2=0.50$ ). This likely indicates that HAND maybe a better indicator to distinguish hydrological  
904 similarity than TWI.

905 For the 323 MOPEX catchments, HSC improved the averaged validation value of  $I_{KGE}$  from 0.62 (HBV) and  
906 0.61 (TOPMODEL) to 0.65. In 12% of the MOPEX catchments, the HSC module outperforms HBV, and in  
907 not a single catchment did the calibrated HBV outperform the HSC. Comparing with TOPMODEL, the HSC  
908 outperformed in 8% of the catchments, and in only 1% of catchments TOPMODEL has a better  
909 performance. ~~Interestingly, we found that the HSC module has showed better performance in the~~  
910 ~~catchments with gentle topography, less forest cover, and a larger aridity index.~~ Not surprisingly, the  $I_{KGE}$   
911 of HSC-MCT model was slightly reduced to 0.59, due to the non-calibrated  $S_{uMax}$ , but still comparably well  
912 performed as HBV (0.62) and TOPMODEL (0.61). This illustrates the robustness of both the HSC approach  
913 to derive the spatial distribution of the root zone storage capacity ( $\beta$ ) and the efficiency of the MCT  
914 method to estimate the root zone storage capacity ( $S_{uMax}$ ).

915

## 916

### 917 Acknowledgement:

918 This study was supported by [National Natural Science Foundation of China \(41801036\)](#), National Key R&D  
919 Program of China (2017YFE0100700), ~~and~~ the Key Program of National Natural Science Foundation of  
920 China (No. 41730646), [and Key Laboratory for Mountain Hazards and Earth Surface Process, Institute of](#)  
921 [Mountain Hazards and Environment, Chinese Academy of Sciences \(KLMHESP-17-02\)](#).

922

## 923 Author contributions:

924 H.G. and H.H.G.S. designed research; H.G. performed research; C.B., C.S., D.T and H.G. provided data,  
925 among which the dynamics of the saturation areas data in the BB was provided by C.B. C.S., and D.T.; H.G.  
926 analysed data; C.B. was involved in the interpretation of some of the modelling work in the BB; H.G. M.H.  
927 and H.H.G.S. wrote the paper; CS and DT extensively edited the paper, and provided substantial comments  
928 and constructive suggestions for scientific clarification.

929

930 **References:**

931 Anderson, M. C., Kustas, W. P., Norman, J. M., Hain, C. R., Mecikalski, J. R., Schultz, L., González-Dugo, M.  
932 P., Cammalleri, C., D'Urso, G., Pimstein, A., and Gao, F.: Mapping daily evapotranspiration at field to  
933 continental scales using geostationary and polar orbiting satellite imagery, *Hydrol. Earth Syst. Sci.*, 15,  
934 223–239, doi:10.5194/hess-15-223-2011, 2011.

935 Andréassian V, Bourgin F, Oudin L, Mathevet T, Perrin C, Lerat J, Coron L, Berthet L.: [2014](#). Seeking  
936 genericity in the selection of parameter sets: Impact on hydrological model efficiency. *Water Resources*  
937 *Research* 50 (10): 8356–8366, [2014](#).

938 Bergström S, Forsman A.: [1973](#). Development of a conceptual deterministic rainfall-runoff model.  
939 *Hydrology Research* 4 (3): 147–170, [1973](#).

940 Bergström S, Lindström G.: [2015](#). Interpretation of runoff processes in hydrological modelling—  
941 experience from the HBV approach. *Hydrological Processes* 29 (16): 3535–3545, [2015](#).

942 Beven K.: [2004](#). Robert E. Horton's perceptual model of infiltration processes. *Hydrological Processes* 18  
943 (17): 3447–3460 DOI: 10.1002/hyp.5740, [2004](#).

944 Beven K, Freer J.: [2001](#). A dynamic TOPMODEL. *Hydrological Processes* 15 (10): 1993–2011 DOI:  
945 10.1002/hyp, [2001](#).

946 Beven K. 1993. Prophecy, reality and uncertainty in distributed hydrological modelling. *Advances in Water*  
947 *Resources* 16 (1): 41–51 DOI: [http://dx.doi.org/10.1016/0309-1708\(93\)90028-E](http://dx.doi.org/10.1016/0309-1708(93)90028-E)

948 Beven K.: [1995](#). Linking parameters across scales: Subgrid parameterizations and scale dependent  
949 hydrological models. *Hydrological Processes* 9 (September 1994): 507–525 DOI:  
950 10.1002/hyp.3360090504.252, [1995](#).

951 Beven KJ.: [2012](#). Rainfall–Runoff Models: The Primer, [2012](#).

952 Beven K., Germann P.: [1982](#). Macropores and water-flow in soils. *Water Resour. Res.* 18, 1311–1325, [1982](#).

953 Beven KJ, Kirkby MJ.: [1979](#). A physically based, variable contributing area model of basin hydrology.  
954 Hydrological Sciences Bulletin 24 (1): 43–69 DOI: 10.1080/02626667909491834, [1979](#).

955 Beven, K.: [1989](#). Changing ideas in hydrology – the case of physically-based models. *J. Hydrol.* 105 (1–2),  
956 157–172, [1989](#).

957 Birkel C, Tetzlaff D, Dunn SM, Soulsby C.: [2010](#). Towards a simple dynamic process conceptualization in  
958 rainfall–runoff models using multi-criteria calibration and tracers in temperate, upland catchments.  
959 *Hydrological Processes* 24 (3): 260–275, [2010](#).

960 Birkel, C., Soulsby, C., and D. Tetzlaff, [\(2014\)](#) Conceptual modelling to assess how the interplay of  
961 hydrological connectivity, catchment storage and tracer dynamics controls non-stationary water age  
962 estimates. *Hydrological Processes*, DOI: 10.1002/hyp.10414, [2014](#).

963 Blöschl G.: [2013](#). Runoff prediction in ungauged basins: synthesis across processes, places and scales.  
964 Cambridge University Press, [2013](#).

965 [Brooks, R. J., Barnard, H. R., Coulombe, R. & McDonnell, J. J.: Ecohydrologic separation of water between](#)  
966 [trees and streams in a Mediterranean climate. \*Nature Geoscience\* 3, 100–104. DOI: 10.1038/geo722,](#)  
967 [2010](#).

968 Budyko MI.: [1971](#). Climate and life, [1971](#).

969 Burt TP, McDonnell JJ.: [2015](#). Whither field hydrology? The need for discovery science and outrageous  
970 hydrological hypotheses. *Water Resources Research* 51 (8): 5919–5928 DOI: 10.1002/2014WR016839,  
971 [2015](#).

972 Chase, CG.: [1992](#). Fluvial landsculpting and the fractal dimension of topography. *Geomorphology* 5 (1):  
973 39–57 DOI: [http://dx.doi.org/10.1016/0169-555X\(92\)90057-U](http://dx.doi.org/10.1016/0169-555X(92)90057-U), [1992](#).

974 Clark, MP, Slater, AG, Rupp, DE, Woods, R [aA.](#), Vrugt, J [aA.](#), Gupta, H V., Wagener, T, Hay, LE.: [2008](#).  
975 Framework for Understanding Structural Errors (FUSE): A modular framework to diagnose differences  
976 between hydrological models. *Water Resources Research* 44: 1–14 DOI: 10.1029/2007WR006735, [2008](#).

977 Clark, [Marty M.](#) P., [Dmitri](#) Kavetski, [D.](#) and [Fabrizio](#) Fenicia, [F.](#): “Pursuing the Method of Multiple Working  
978 Hypotheses for Hydrological Modeling.” *Water Resources Research* 47.9 ([2011](#)): 1–16, [2011](#).

979 Colombo, R., Vogt, J.-V., Soille, P., Paracchini, M. L., de Jager, A.: 2007. Deriving river networks and  
980 catchments at the European scale from medium resolution digital elevation data. *CATENA* 70 (3): 296–  
981 305 DOI: <http://doi.org/10.1016/j.catena.2006.10.001>, 2007.

982 Condon, Laura E, and Reed M Maxwell. "Evaluating the Relationship between Topography and  
983 Groundwater Using Outputs from a Continental-Scale Integrated Hydrology Model." *Water Resources*  
984 *Research* 51.8 (2015): 6602–6621.

985 Duan, Q., Schaake, J., Andréassian, V., Franks, S., Goteti, G., Gupta, H. V., Gusev, YM, Habets, F., Hall, A.,  
986 Hay, L., et al. 2006. Model Parameter Estimation Experiment (MOPEX): An overview of science strategy  
987 and major results from the second and third workshops. *Journal of Hydrology* 320 (1-2): 3–17 DOI:  
988 10.1016/j.jhydrol.2005.07.031, 2006.

989 Dunne, T., Black, R. D.: 1970. Partial area contributions to Storm Runoff in a Small New England Watershed.  
990 *Water Resources Research* 6 (5): 1296–1311, 1970.

991 Boer-Euser, T., H. K. McMillan, H. K., M. Hrachowitz, M., H. C. Winsemius, H. C., and H. H. G. Savenije, H.  
992 H. G.: (2016), Influence of soil and climate on root zone storage capacity, *Water Resour. Res.*, 52, 2009–  
993 2024, doi:10.1002/2015WR018115, 2016.

994 Fan, Y., Miguez macho, G., Jobbág, E. G., Jackson, R. B., & Oterocasal, C.: (2017) Hydrologic regulation of  
995 plant rooting depth. *Proceedings of the National Academy of Sciences of the United States of America*,  
996 114(40), 201712381, 2017.

997 Fenicia, F., Savenije, H. H. G., Matgen, P., Pfister, L.: 2007. A comparison of alternative multiobjective  
998 calibration strategies for hydrological modeling. *Water Resources Research* 43 (3): n/a–n/a DOI:  
999 10.1029/2006WR005098, 2007.

1000 Gao, H., Hrachowitz, M., Schymanski, S. J., Fenicia, F., Sriwongsitanon, N., Savenije, H. H. G.: 2014a. Climate  
1001 controls how ecosystems size the root zone storage capacity at catchment scale. *Geophysical Research*  
1002 Letters 41 (22): 7916–7923 DOI: 10.1002/2014gl061668, 2014a.

1003 Gao, H., Hrachowitz, M., Fenicia, F., Gharari, S., Savenije, H. H. G.: 2014b. Testing the realism of a  
1004 topography-driven model (FLEX-Topo) in the nested catchments of the Upper Heihe, China. *Hydrology*  
1005 and Earth System Sciences

1006 Gao, H., Hrachowitz, M., Sriwongsitanon, N., Fenicia, F., Gharari, S., Savenije, H.H.G.: 2016. Accounting for  
1007 the influence of vegetation and landscape improves model transferability in a tropical savannah region.  
1008 Water Resources Research 52 (10): 7999–8022 DOI: 10.1002/2016WR019574, 2016.

1009 Gao, H., Cai, H., Zheng, D.: 2017. Understand the impacts of landscape features on the shape of storage  
1010 capacity curve and its influence on flood. Hydrology Research. DOI: Hydrology-D-16-00245R3 Gao, H., Sabo,  
1011 J.L., Chen, X., Liu, Z., Yang, Z., Ren, Z., Liu, M.: Landscape heterogeneity and hydrological processes: a  
1012 review of landscape-based hydrological models. Landscape Ecology, DOI: doi.org/10.1007/s10980-018-  
1013 0690-4, 2018a.

1014 Gao, H., Cai, H., Zheng, D.: 2017. Understand the impacts of landscape features on the shape of storage  
1015 capacity curve and its influence on flood. Hydrology Research. DOI: Hydrology-D-16-00245R3, 2018b.

1016 Gao, J., Holden, J., Kirkby, M.: 2016. The impact of land-cover change on flood peaks in peatland basins.  
1017 Water Resources Research 52 (5): 3477–3492 DOI: 10.1002/2015WR017667, 2016.

1018 Gharari, S., Hrachowitz, M., Fenicia, F., Savenije, H.H.G.: 2011. Hydrological landscape classification:  
1019 investigating the performance of HAND based landscape classifications in a central European meso-scale  
1020 catchment. Hydrology and Earth System Sciences 15 (11): 3275–3291 DOI: 10.5194/hess-15-3275-2011,  
1021 2011.

1022 Gharari, S., Hrachowitz, M., Fenicia, F., Gao, H., Savenije, H.H.G.: 2014. Using expert knowledge to increase  
1023 realism in environmental system models can dramatically reduce the need for calibration. Hydrology and  
1024 Earth System Sciences 18 (12): 4839–4859 DOI: 10.5194/hess-18-4839-2014, 2014.

1025 Gharari, S. On the role of model structure in hydrological modeling: Understanding models, PhD  
1026 dissertation, 2016

1027 Gomes, G.J.C., Vrugt, J.A., Vargas, E.A.: 2016. Toward improved prediction of the bedrock depth  
1028 underneath hillslopes: Bayesian inference of the bottom-up control hypothesis using high-resolution  
1029 topographic data. Water Resources Research 52 (4): 3085–3112 DOI: 10.1002/2015WR018147, 2016.

1030 Grabs, T., Seibert, J., Bishop, K., Laudon, H.: 2009. Modeling spatial patterns of saturated areas: A  
1031 comparison of the topographic wetness index and a dynamic distributed model. Journal of Hydrology 373  
1032 (1): 15–23, 2009.

1033 De Groen, M.M., Savenije, H.H.G.: [2006](#). A monthly interception equation based on the statistical  
1034 characteristics of daily rainfall. *Water Resources Research* 42 (12): n/a–n/a DOI: 10.1029/2006WR005013, [2006](#).

1035

1036 Gumbel, E. J.: [\(1935\)](#), Les valeurs extrêmes des distributions statistiques, *Annales de l'institut Henri  
1037 Poincaré*, 5(2), 115–158, [1935](#).

1038 Gupta, H. V., Kling, H., Yilmaz, K.K., Martinez, G.F.: [2009](#). Decomposition of the mean squared error and  
1039 NSE performance criteria: Implications for improving hydrological modelling. *Journal of Hydrology* 377 (1-  
1040 2): 80–91 DOI: 10.1016/j.jhydrol.2009.08.003, [2009](#).

1041 Hargreaves, G.H., Samani, Z.A.: [1985](#). Reference crop evapotranspiration from temperature. *Applied  
1042 engineering in agriculture* 1 (2): 96–99, [1985](#).

1043 Haria, A.H., Shand, P.: [2004](#). Evidence for deep sub-surface flow routing in forested upland Wales:  
1044 implications for contaminant transport and stream flow generation. *Hydrology and Earth System Sciences  
1045 Discussions* 8 (3): 334–344, [2004](#).

1046 Harte, J.: [2002](#). Toward a synthesis of the Newtonian and Darwinian worldviews. *Physics Today* 55 (10):  
1047 29–34 DOI: 10.1063/1.1522164, [2002](#).

1048 Helmlinger, K.R., Kumar, P., Foufoula-Georgiou, E.: [1993](#). On the use of digital elevation model data for  
1049 Hortonian and fractal analyses of channel network. *Water Resources Research* 29: 2599–2613, [1993](#).

1050 Hewlett, J.D.: [1961](#). Soil moisture as a source of base flow from steep mountain watersheds. *Southeastern  
1051 Forest Experiment Station, US Department of Agriculture, Forest Service*, [1961](#).

1052 Hewlett, J.D., Troendle, C.A.: [1975](#). Non point and diffused water sources: a variable source area problem.  
1053 In *Watershed Management; Proceedings of a Symposium*, [1975](#).

1054 [Homer, C. G., Dewitz, J. A., Yang, L., Jin, S., Danielson, P., Xian, G., Coulston, J., Herold, N. D., Wickham, J.  
1055 D. & Megown, K.: Completion of the 2011 National Land Cover Database for the conterminous United  
1056 States-representing a decade of land cover change information. Photogrammetric Engineering and  
1057 Remote Sensing](#) 81, 345–354, [2015](#).

1058 Hooshyar, M., Wang, D., Kim, S., Medeiros, S.C., Hagen, S.C.: [2016](#). Valley and channel networks extraction  
1059 based on local topographic curvature and k-means clustering of contours. *Water Resources Research* 52  
1060 (10): 8081–8102, [2016](#).

1061 Horton, R.E.: [1933](#). The role of infiltration in the hydrologic cycle. *Trans. Am. Geophys. Union* 14, 446–  
1062 460, [1933](#).

1063 Hrachowitz, M., Savenije, H.H.G., Blöschl, G., McDonnell, J.J., Sivapalan, M., Pomeroy, J.W., Arheimer, B.,  
1064 Blume, T., Clark, M.P., Ehret, U., Fenicia, F., Freer, J.E., Gelfan, A., Gupta, H.V., Hughes, D.A., Hut, R.W.,  
1065 Montanari, A., Pande, S., Tetzlaff, D., Troch, P.A., Uhlenbrook, S., Wagener, T., Winsemius, H.C., Woods,  
1066 R.A., Zehe E., & Cudennec, C.: [et al. 2013](#). A decade of Predictions in Ungauged Basins (PUB)—a review.  
1067 *Hydrological Sciences Journal* 58 (6): 1198–1255 DOI: 10.1080/02626667.2013.803183, [2013](#).

1068 Hu, G. and Jia, L.: Monitoring of evapotranspiration in a semiarid inland river basin by combining  
1069 microwave and optical remote sensing observations, *Remote Sens.*, 7, 3056–3087,  
1070 doi:10.3390/rs70303056, 2015.

1071 Iorgulescu, I., Jordan, J-P.: [1994](#). Validation of TOPMODEL on a small Swiss catchment. *Journal of  
1072 Hydrology* 159 (1): 255–273 DOI: [http://dx.doi.org/10.1016/0022-1694\(94\)90260-7](http://dx.doi.org/10.1016/0022-1694(94)90260-7), [1994](#).

1073 Kirchner, J.W.: [2006](#). Getting the right answers for the right reasons: Linking measurements, analyses, and  
1074 models to advance the science of hydrology. *Water Resources Research* 42 (3): n/a–n/a DOI:  
1075 10.1029/2005WR004362, [2006](#).

1076 Kleidon, A., Lorenz, R.D.: [2004](#). Non-equilibrium thermodynamics and the production of entropy: life,  
1077 earth, and beyond. *Springer Science & Business Media*, [2004](#).

1078 Kollat, J. B., P. M. Reed, and T. Wagener.: “When are multiobjective calibration trade - offs in hydrologic  
1079 models meaningful?.” *Water Resources Research* 48.3([2012](#)):3520, [2012](#).

1080 Liang, X., Lettenmaier, D.P., Wood, E.F., Burges, S.J.: [1994](#). A simple hydrologically based model of land  
1081 surface water and energy fluxes for general circulation models. *Journal of Geophysical Research* 99 (D7):  
1082 14415 DOI: 10.1029/94JD00483, [1994](#).

1083 Liu, D., Tian, F., Hu, H., Hu, H.: [2012](#). The role of run-on for overland flow and the characteristics of runoff  
1084 generation in the Loess Plateau, China. *Hydrological Sciences Journal* 57 (6): 1107–1117 DOI:  
1085 10.1080/02626667.2012.695870, [2012](#).

1086 Maxwell, [Reed R.](#) M., and [Laura E.](#) Condon, [L. E.](#): “Connections between Groundwater Flow and  
1087 Transpiration Partitioning.” *Science* 353.6297 ([2016](#)): 377 LP – 380, [2016](#).

1088 McDonnell, J.J., Sivapalan, M., Vaché, K., Dunn, S., Grant, G., Haggerty, R., Hinz, C., Hooper, R., Kirchner, J., Roderick, M.L., Selker, J. and Weiler, M.:et al. 2007. Moving beyond heterogeneity and process complexity: A new vision for watershed hydrology. *Water Resources Research* 43 (7): n/a–n/a DOI: 10.1029/2006WR005467, [2007](#).

1092 McDonnell, J.J.: [2013](#). Are all runoff processes the same? *Hydrological Processes* 27 (26): 4103–4111 DOI: 10.1002/hyp.10076, [2013](#).

1094 Merz, R., Blöschl, G.: [2004](#). Regionalisation of catchment model parameters. *Journal of Hydrology* 287 (1-4): 95–123 DOI: 10.1016/j.jhydrol.2003.09.028, [2004](#).

1096 Milly, P. C. D.: [\(1994\)](#). Climate, soil water storage, and the average annual water balance, *Water Resour. Res.*, 30(7), 2143–2156, [1994](#).

1098 Molenat, J., Gascuel-Odoux, C., Ruiz, L., Gruau, G.: [2008](#). Role of water table dynamics on stream nitrate export and concentration in agricultural headwater catchment (France). *Journal of Hydrology* 348 (3): 363–378, [2008](#).

1101 Molénat, J., Gascuel-Odoux, C., Davy, P., Durand, P.: [2005](#). How to model shallow water-table depth variations: the case of the Kervidy-Naizin catchment, France. *Hydrological Processes* 19 (4): 901–920, [2005](#).

1103 Montgomery, D.R., Dietrich, W.E.: [1989](#). Source areas, drainage density, and channel initiation. *Water Resources Research* 25 (8): 1907–1918, [1989](#).

1105 Moore, R. J.: [\(1985\)](#). The probability-distributed principle and runoff production at point and basin scales, *Hydrol. Sci. J.*, 30, 273-297, [1985](#).

1107 Moussa, R.: [2008](#). Effect of channel network topology, basin segmentation and rainfall spatial distribution on the geomorphologic instantaneous unit hydrograph transfer function. *Hydrological Processes* 22 (3): 395–419 DOI: 10.1002/hyp.6612, [2008](#).

1110 Moussa, R.: [2009](#). Definition of new equivalent indices of Horton-Strahler ratios for the derivation of the Geomorphological Instantaneous Unit Hydrograph. *Water Resources Research* 45 (9): n/a–n/a DOI: 10.1029/2008WR007330, [2009](#).

1113 Nobre, A. D., Cuartas, L. A., Hodnett, M., Rennó, C. D., Rodrigues, G., Silveira, A., Waterloo, M., Saleska, S.: [2011](#). Height Above the Nearest Drainage - a hydrologically relevant new terrain model. *Journal of Hydrology* 404 (1-2): 13–29 DOI: 10.1016/j.jhydrol.2011.03.051, [2011](#).

1116 Orth, R., Staudinger, M., Seneviratne, S.I., Seibert, J., Zappa, M.: [2015](#). Does model performance improve  
1117 with complexity? A case study with three hydrological models. *Journal of Hydrology* 523: 147–159 DOI:  
1118 <http://doi.org/10.1016/j.jhydrol.2015.01.044>, [2015](#).

1119 Passalacqua, P., Belmont, P., Staley, D.M., Simley, J.D., Arrowsmith, J.R., Bode, C.A., Crosby, C., DeLong,  
1120 S.B., Glenn, N.F., Kelly, S.A., [Lague, D.](#), [Sangireddy, H.](#), [Schaffrath, K.](#), [Tarboton, D. G.](#), [Wasklewicz, T.](#),  
1121 [Wheaton, J. M.](#): [et al. 2015](#). Analyzing high resolution topography for advancing the understanding of mass  
1122 and energy transfer through landscapes: A review. *Earth-Science Reviews* 148: 174–193 DOI:  
1123 <http://doi.org/10.1016/j.earscirev.2015.05.012>, [2015](#).

1124 Pelletier, J.D., Barron-Gafford, G.A., Breshears, D.D., Brooks, P.D., Chorover, J., Durcik, M., Harman, C.J.,  
1125 Huxman, T.E., Lohse, K.A., Lybrand, R., [Meixner, T.](#), [McIntosh, J. C.](#), [Papuga, S. A.](#), [Rasmussen, C.](#), [Schaap,](#)  
1126 [M.](#), [Swetnam, T. L.](#), and [Troch, P. A.](#): [et al. 2013](#). Coevolution of nonlinear trends in vegetation, soils, and  
1127 topography with elevation and slope aspect: A case study in the sky islands of southern Arizona. *Journal*  
1128 of *Geophysical Research: Earth Surface* 118 (2): 741–758 DOI: 10.1002/jgrf.20046, [2013](#).

1129 Perrin, C., Michel, C., Andréassian, V.: [2001](#). Does a large number of parameters enhance model  
1130 performance? Comparative assessment of common catchment model structures on 429 catchments.  
1131 *Journal of Hydrology* 242 (3-4): 275–301 DOI: 10.1016/S0022-1694(00)00393-0, [2001](#).

1132 [Perrin, C., C. Michel, and V. Andre'assian: Improvement of a parsimonious model for streamflow](#)  
1133 [simulation, J. Hydrol., 279, 275– 289, 2003.](#)

1134 Ponce, V. M., and [R. H. Hawkins, R. H.](#): [\(1996\)](#). Runoff curve number: Has it reached maturity?, *J. Hydrol.*  
1135 Eng., 1(1), 11–19, [1996](#).

1136 Rempe, D. M., and [W. E. Dietrich, W. E.](#): [\(2014\)](#). A bottom-up control on fresh-bedrock topography under  
1137 landscapes, *Proc. Natl. Acad. Sci. U. S. A.*, 111(18), 6576–6581, doi:10.1073/pnas.1404763111, [2014](#).

1138 [Renard, K. G., Yoder, D. C., Lightle, D. T. & Dabney, S. M. Universal soil loss equation and revised universal](#)  
1139 [soil loss equation. Handbook of Erosion Modelling 8, 135–167, 2011.](#)

1140 Rennó, C.D., Nobre, A.D., Cuartas, L.A., Soares, J.V., Hodnett, M.G., Tomasella, J., Waterloo, M., [2008](#).  
1141 HAND, a new terrain descriptor using SRTM-DEM; mapping terra-firme rainforest environments in  
1142 Amazonia. *Remote Sensing of Environment* 112, 3469–3481, [2008](#).

1143 Rodriguez-Iturbe, I., and A. Rinaldo, Fractal River Basins: Chance and Self-Organization, Cambridge Univ.  
1144 Press, 547 pp., New York, 1997.

1145 Samaniego, L., Kumar, R., Attinger, S.: 2010. Multiscale parameter regionalization of a grid-based  
1146 hydrologic model at the mesoscale. *Water Resources Research* 46 (5): n/a–n/a DOI:  
1147 10.1029/2008WR007327, 2010.

1148 Savenije, H. H. G.: HESS Opinions “Topography driven conceptual modelling (FLEX-Topo)”, *Hydrol. Earth  
1149 Syst. Sci.*, 14, 2681–2692, doi:10.5194/hess-14-2681-2010, 2010.

1150 Savenije, H. H. G., Hrachowitz, M.: 2017. HESS Opinions ‘Catchments as meta-organisms – a new blueprint  
1151 for hydrological modelling’. *Hydrol. Earth Syst. Sci.* 21 (2): 1107–1116 DOI: 10.5194/hess-21-1107-2017,  
1152 2017.

1153 Schaake, J., S.-Cong, S., and Q.-Duan, Q.: (2006). The US MOPEX data set, IAHS Publ., 307, 9, 2006.

1154 Schwarz, G. E. & Alexander, R. B. *State Soil Geographic (STATSGO) Data Base for the Conterminous United  
1155 States. Open File report 95-449, US Geological Survey, Washington, DC, 1995.*

1156 Seibert, J., Stendahl, J., Sørensen, R.: 2007. Topographical influences on soil properties in boreal forests.  
1157 *Geoderma* 141 (1-2): 139–148 DOI: 10.1016/j.geoderma.2007.05.013, 2007.

1158 Shao, W., Su, Y., and Langhammer, J.: *Simulations of coupled non-isothermal soil moisture transport and  
1159 evaporation fluxes in a forest area. Journal of Hydrology and Hydromechanics*, 65, 410–425, 2018

1160

1161 Shand, P., Haria, A. H., Neal, C., Griffiths, L., Gooddy, D., Dixon, A. J., Hill, T., Buckley, D. K., Cunningham, J.:  
1162 2005. Hydrochemical heterogeneity in an upland catchment: further characterisation of the spatial,  
1163 temporal and depth variations in soils, streams and groundwaters of the Plynlimon forested catchment,  
1164 Wales. *Hydrology and Earth System Sciences* 9 (6): 621–644, 2005.

1165 Sørensen, R., Seibert, J.: 2007. Effects of DEM resolution on the calculation of topographical indices: TWI  
1166 and its components. *Journal of Hydrology* 347 (1): 79–89 DOI:  
1167 <http://dx.doi.org/10.1016/j.jhydrol.2007.09.001>, 2007.

1168 Sivapalan, M., Woods, R. A., Kalma, J. D.: 1997. Variable bucket representation of TOPMODEL and  
1169 investigation of the effects of rainfall heterogeneity. *Hydrological processes* 11 (9): 1307–1330, 1997.

1170 Sivapalan, M., Takeuchi, K., Franks, S. W., Gupta, V. K., Karambiri, H., Lakshmi, V., Liang, X., McDonnell, J. J.,  
1171 Mendiondo, E. M., O'Connell, P. E., et al. Oki, T., Pomeroy, J. W., Schertzer, D., Uhlenbrook, S., Zehe, E.:  
1172 2003. IAHS Decade on Predictions in Ungauged Basins (PUB), 2003–2012: Shaping an exciting future for  
1173 the hydrological sciences. *Hydrological Sciences Journal* 48 (6): 857–880 DOI:  
1174 10.1623/hysj.48.6.857.51421, 2003.

1175 Sivapalan, M.: 2009. The secret to 'doing better hydrological science': change the question! *Hydrological  
1176 Processes* 23 (9): 1391–1396 DOI: 10.1002/hyp.7242, 2009.

1177 Sivapalan, M., Blöschl, G.: 2015. Time scale interactions and the coevolution of humans and water. *Water  
1178 Resources Research* 51 (9): 6988–7022 DOI: 10.1002/2015WR017896, 2015.

1179 Soulsby, C., Birkel, C., Geris, J., Dick, J., Tunaley, C. and Tetzlaff, D.: (2015) Stream water age distributions  
1180 controlled by storage dynamics and non-linear hydrologic connectivity: modelling with high resolution  
1181 isotope data. *Water Resources Research*. DOI: 10.1002/2015WR017888, 2015.

1182 Soulsby, C., Bradford, J., Dick, J., McNamara, J. P., Geris, J., Lessels, J., Blumstock, M., Tetzlaff, D.: 2016.  
1183 Using geophysical surveys to test tracer-based storage estimates in headwater catchments. *Hydrological  
1184 Processes* 30 (23): 4434–4445 DOI: 10.1002/hyp.10889, 2016.

1185 Sklash, M. G., Farvolden, R. N.: 1979. The role of groundwater in storm runoff. *Journal of Hydrology* 43 (1):  
1186 45–65 DOI: [http://dx.doi.org/10.1016/0022-1694\(79\)90164-1](http://dx.doi.org/10.1016/0022-1694(79)90164-1), 1979.

1187 Tetzlaff, D., Birkel, C., Dick, J., and C. Soulsby: (2014) Storage dynamics in hydromedical units control  
1188 hillslope connectivity, runoff generation and the evolution of catchment transit time distributions. *Water  
1189 Resources Research*, DOI: 10.1002/2013WR014147, 2014.

1190 Tian, F. Q., Hu, H. P., & Lei, Z. D.: *Thermodynamic watershed hydrological model: constitutive relationship.*  
1191 *Science in China Series E: Technological Sciences*, 51(9), 1353-1369, 2008.

1192 Troch, P. A., Carrillo, G., Sivapalan, M., Wagener, T., Sawicz, K.: 2013. Climate-vegetation-soil interactions  
1193 and long-term hydrologic partitioning: signatures of catchment co-evolution. *Hydrology and Earth System  
1194 Sciences* 17 (6): 2209–2217 DOI: 10.5194/hess-17-2209-2013, 2013.

1195 Tromp-van Meerveld, H. J. & McDonnell, J. J.: *Threshold relations in subsurface stormflow: 1. A 147-storm  
1196 analysis of the Panola hillslope.* *Water Resources Research* 42. DOI: 10.1029/2004WR003778, 2006.

1197 Van Beek, L.P.H. and M.F.P. Bierkens (2008), The Global Hydrological Model PCR-GLOBWB:  
1198 Conceptualization, Parameterization and Verification, Report Department of Physical Geography, Utrecht  
1199 University, Utrecht, The Netherlands, <http://vanbeek.geo.uu.nl/suppinfo/vanbeekbierkens2009.pdf>,  
1200 2008.

1201 Vrugt, J. A.: 2003. Effective and efficient algorithm for multiobjective optimization of hydrologic models.  
1202 Water Resources Research 39 (8): 1–19 DOI: 10.1029/2002WR001746, 2003.

1203 Wang, D., Tang, Y.: 2014. A one-parameter Budyko model for water balance captures emergent behavior  
1204 in darwinian hydrologic models. Geophysical Research Letters 41 (13): 4569–4577, 2014.

1205 Wang, D.: A new probability density function for spatial distribution of soil water storage capacity leads  
1206 to SCS curve number method, Hydrol. Earth Syst. Sci. Discuss., <https://doi.org/10.5194/hess-2018-32>, in  
1207 review, 2018.

1208 Wang-Erlandsson, L., Bastiaanssen, W.G.M., Gao, H., Jägermeyr, J., Senay, G.B., van Dijk, A.I.J.M.,  
1209 Guerschman, J.P., Keys, P.W., Gordon, L.J., Savenije, H.H.G.: 2016. Global root zone storage capacity from  
1210 satellite-based evaporation. Hydrol. Earth Syst. Sci. 20 (4): 1459–1481 DOI: 10.5194/hess-20-1459-2016,  
1211 2016.

1212 Weiler, M., McDonnell, J. J.: 2007. Conceptualizing lateral preferential flow and flow networks and  
1213 simulating the effects on gauged and ungauged hillslopes. Water Resour. Res. 43, W03403, 2007.

1214 Wolock, D. M.: STATSGO Soil Characteristics for the Conterminous United States. US Geological Survey,  
1215 Washington, DC., 1997.

1216 Ye, A., Duan, Q., Yuan, X., Wood, E.F., Schaake, J.: 2014. Hydrologic post-processing of MOPEX streamflow  
1217 simulations. Journal of Hydrology 508: 147–156 DOI: 10.1016/j.jhydrol.2013.10.055, 2014.

1218 Yu, Z., Lu, Q., Zhu, J., Yang, C., Ju, Q., Yang, T., Chen, X., and Sudicky, E. A.: Spatial and temporal scale effect  
1219 in simulating hydrologic processes in a watershed. Journal of Hydrologic Engineering, 19(1), 99-107, 2014.

1220 Zehe, E., Fluehler, H.: 2001. Preferential transport of Isoproturon at a plot scale and a field scale tile-  
1221 drained site. J. Hydrol. 247, 100–115, 2001.

1222 Zehe, E., Ehret, U., Blume, T., Kleidon, A., Scherer, U., Westhoff, M.: 2013. A thermodynamic approach to  
1223 link self-organization, preferential flow and rainfall-runoff behaviour. Hydrol. Earth Syst. Sci. 17 (11):  
1224 4297–4322 DOI: 10.5194/hess-17-4297-2013, 2013.

1225 Zhao, R-J., Zuang, Y., Fang, L., Liu, X., Zhang, Q.: 1980. The Xinanjiang model. Hydrological forecasting —  
1226 Prévisions hydrologiques 1980 (129): 351–356, 1980.

1227

1228

1229 Table 1. The parameters of the models, and their prior ranges for calibration. (\* $S_{uMax}$  is a parameter in HBV,  
 1230 TOPMODEL and the HSC model, but HSC-MCT model does not have  $S_{uMax}$  as a free parameter; \*\*  $\beta$  is a parameter in  
 1231 HBV model, but not in TOPMODEL, HSC and HSC-MCT models)

Parameter	Explanation	Prior range for calibration
$S_{iMax}$ (mm)	Maximum interception capacity	2
$S_{uMax}$ (mm)*	The root zone storage capacity	(10, 1000)
$\beta$ (-)**	The shape of the storage capacity curve	(0.01, 5)
$C_e$ (-)	Soil moisture threshold for reduction of evaporation	(0.1, 1)
$D$ (-)	Splitter to fast and slow response reservoirs	(0, 1)
$T_{lagF}$ (d)	Lag time from rainfall to peak flow	(0, 10)
$K_f$ (d)	The fast recession coefficient	(1, 20)
$K_s$ (d)	The slow recession coefficient	(20, 400)

1232

1233

1234 Table 2. The water balance and constitutive equations used in models. (Function (15)\* is used in the HBV model, but  
 1235 not used in the TOPMODEL, HSC and HSC-MCT models)

reservoirs	Water balance equations	Constitutive equations
Interception reservoir	$\frac{dS_i}{dt} = P - E_i - P_e \quad (8)$	$E_i = \begin{cases} E_p; S_i > 0 \\ 0; S_i = 0 \end{cases} \quad (9)$
Unsaturated reservoir	$\frac{dS_u}{dt} = P_e - E_a - R_u \quad (11)$	$P_e = \begin{cases} 0; & S_i < S_{iMax} \\ P; & S_i = S_{iMax} \end{cases} \quad (10)$

---


$$\frac{E_a}{E_p - E_i} = \frac{S_u}{C_e S_{uMax}} \quad (13)$$

Splitter and  
Lag function

$$R_f = R_u D \quad (17); \quad R_s = R_u (1 - D) \quad (14)$$

$$R_{fl}(t) = \sum_{i=1}^{T_{lagf}} c_f(i) \cdot R_f(t-i+1) \quad (15)$$

$$c_f(i) = i / \sum_{u=1}^{T_{lagf}} u \quad (16)$$

Fast reservoir  $\frac{dS_f}{dt} = R_f - Q_f \quad (17)$   $Q_f = S_f / K_f \quad (18)$

Slow reservoir  $\frac{dS_s}{dt} = R_s - Q_s \quad (19)$   $Q_s = S_s / K_s \quad (20)$

---

1236

1237

Table 3. Data source of the MOPEX catchments.

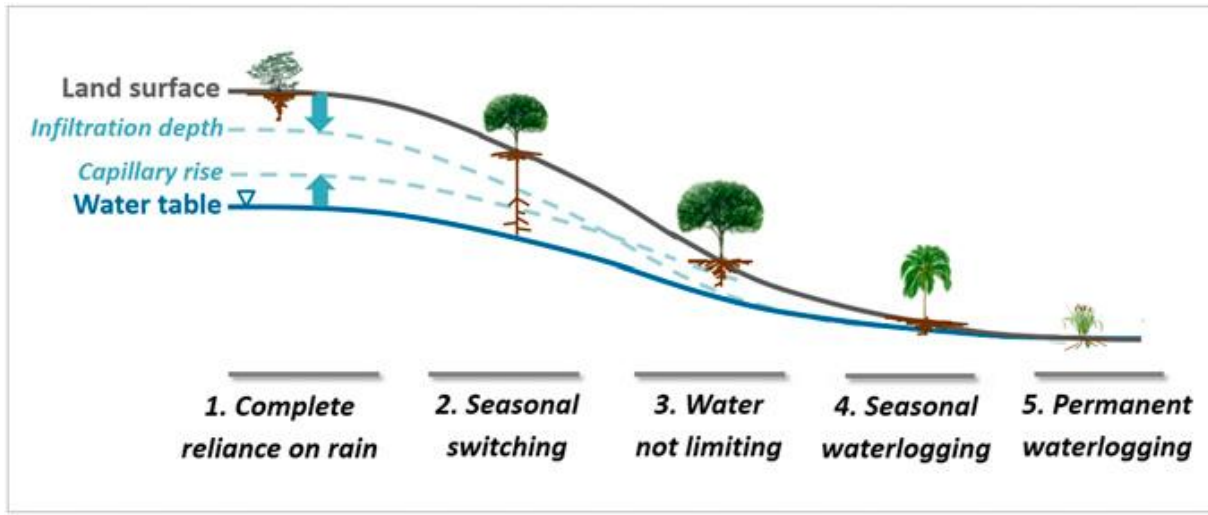
Data	Unit	Resources	Website	Reference
Daily precipitation	mm/d	MOPEX	<a href="http://www.nws.noaa.gov/oh/d/mopex/mo_datasets.htm">http://www.nws.noaa.gov/oh/d/mopex/mo_datasets.htm</a>	(Duan et al., 2006)
Daily maximum temperature	°C	MOPEX	Same as above	Same as above
Daily minimum temperature	°C	MOPEX	Same as above	Same as above
Daily runoff	mm/d	MOPEX	Same as above	Same as above
Aridity index	-	MOPEX	Same as above	Same as above
DEM	m	USGS	<a href="http://earthexplorer.usgs.gov/">http://earthexplorer.usgs.gov/</a>	-
Slope	degree	USGS	Same as above	-
K factor of soil	-	USGS	<a href="http://water.usgs.gov/GIS/metadata/usgswrd/XML/muid.xml">http://water.usgs.gov/GIS/metadata/usgswrd/XML/muid.xml</a>	(Wolock, 1997; Gao et al., 2018)
Percentage of forest cover	%	NLCD	<a href="http://www.mrlc.gov/">http://www.mrlc.gov/</a>	(Homer et al., 2015; Gao et al., 2018)
Stream density	Km/km <sup>2</sup>	Horizon Systems Corporation	<a href="http://www.horizon-systems.com/nhdplus/">http://www.horizon-systems.com/nhdplus/</a>	-

Depth to bedrock      cm      STATSGO      [http://www.soilinfo.psu.edu/index.cgi?soil\\_data&conus&data\\_code&dtb](http://www.soilinfo.psu.edu/index.cgi?soil_data&conus&data_code&dtb)      (Schwarz et al., 1995; Gao et al., 2018)

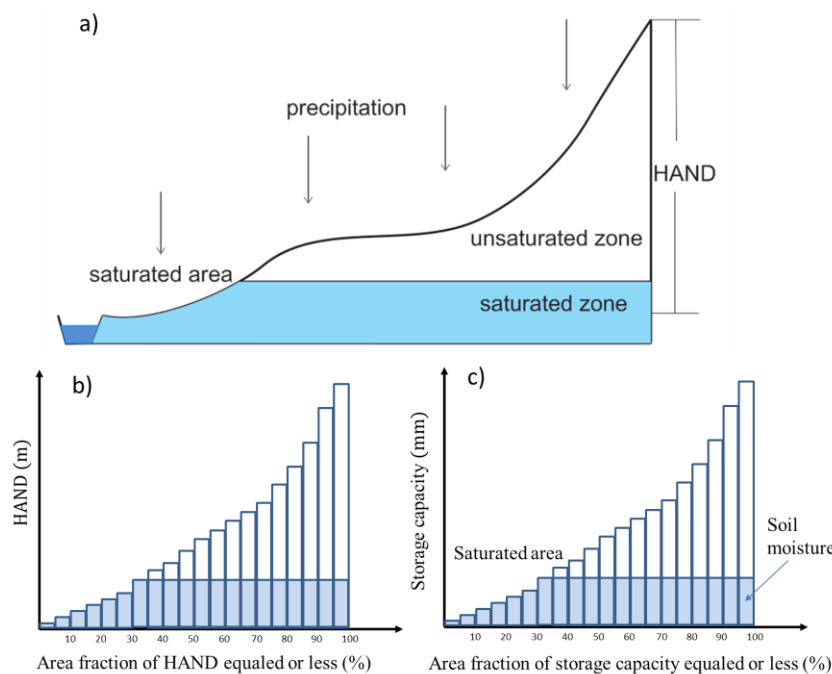
1238  
1239  
1240 Table 4. Impacts of MOPEX catchment characteristics on model performance (HSC, HBV, and TOPMODEL)

<u>Catchment characteristics</u>	<u>HSC &gt; HBV</u>	<u>HSC ≈ HBV</u>	<u>HSC &lt; HBV</u>	<u>HSC &gt; TOPMODEL</u>	<u>HSC ≈ TOPMODEL</u>	<u>HSC &lt; TOPMODEL</u>
<u>Averaged</u>						
<u>HAND (m)</u>	<u>37</u>	<u>71</u>	<u>-</u>	<u>27</u>	<u>69</u>	<u>193</u>
<u>Averaged slope</u>						
<u>(degree)</u>	<u>4.0</u>	<u>5.7</u>	<u>-</u>	<u>3.6</u>	<u>5.6</u>	<u>13.5</u>
<u>Averaged</u>						
<u>elevation (m)</u>	<u>454</u>	<u>395</u>	<u>-</u>	<u>469</u>	<u>393</u>	<u>740</u>
<u>Averaged K-factor (-)</u>						
<u>K-factor (-)</u>	<u>0.28</u>	<u>0.29</u>	<u>-</u>	<u>0.29</u>	<u>0.29</u>	<u>0.25</u>
<u>Forest</u>						
<u>proportion (%)</u>	<u>22</u>	<u>43</u>	<u>-</u>	<u>14</u>	<u>43</u>	<u>68</u>
<u>Aridity index (-)</u>						
<u>Aridity index (-)</u>	<u>1.1</u>	<u>0.9</u>	<u>-</u>	<u>1.3</u>	<u>0.9</u>	<u>0.8</u>
<u>Stream density</u>						
<u>(-)</u>	<u>0.72</u>	<u>0.81</u>	<u>-</u>	<u>0.77</u>	<u>0.80</u>	<u>0.83</u>
<u>Averaged</u>						
<u>depth to rock</u>						
<u>(cm)</u>	<u>192</u>	<u>219</u>	<u>-</u>	<u>210</u>	<u>215</u>	<u>333</u>

1241

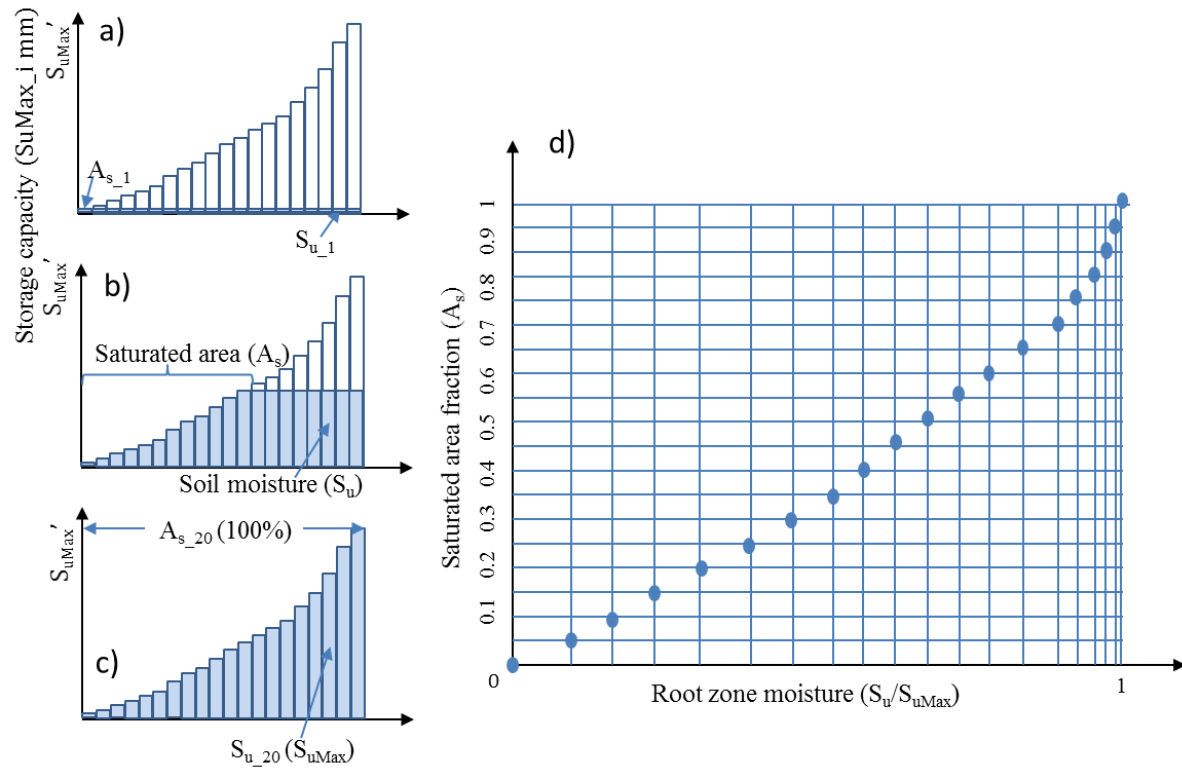


1242  
1243 **Figure 1.** The variation of plant rooting depths along a hillslope profile, showing the impact of HAND  
1244 (Height Above the Nearest Drainage) on rooting depth. (Taken from Fan et al., 2017 by permission of PNAS)



1245  
1246 Figure 24. The perceptual model of the HAND-based Storage Capacity curve (HSC) model. a) shows the  
1247 representative hillslope profile in nature, and the saturated area, unsaturated zone and saturated zone; b) shows  
1248 the relationship between HAND bands and their corresponded area fraction; c) shows the relationship between  
1249 storage capacity-area fraction-soil moisture-saturated area, based on the assumption that storage capacity linearly  
1250 increases with HAND values.

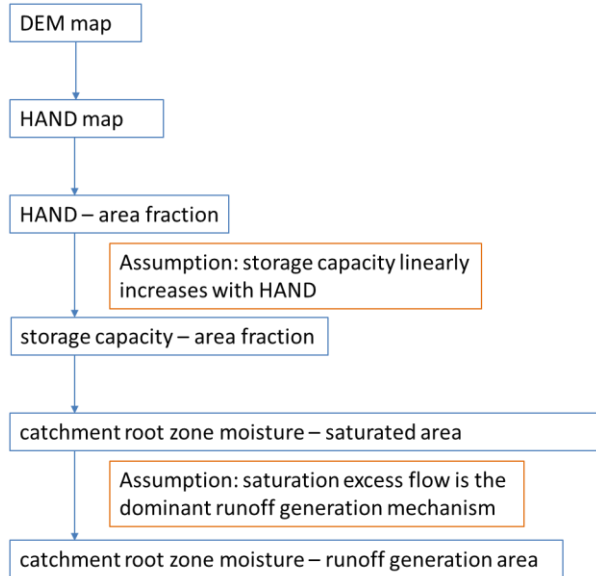
1252



1253

1254 Figure 23. The conceptual model of the HSC model. a), b) and c) illustrate the relationship between soil moisture ( $S_u$ )  
1255 and saturated area ( $A_s$ ) in different soil moisture conditions. In d), 20 different  $S_u$ - $A_s$  conditions are plotted, which  
1256 allow us to estimate  $A_s$  from  $S_u$ .

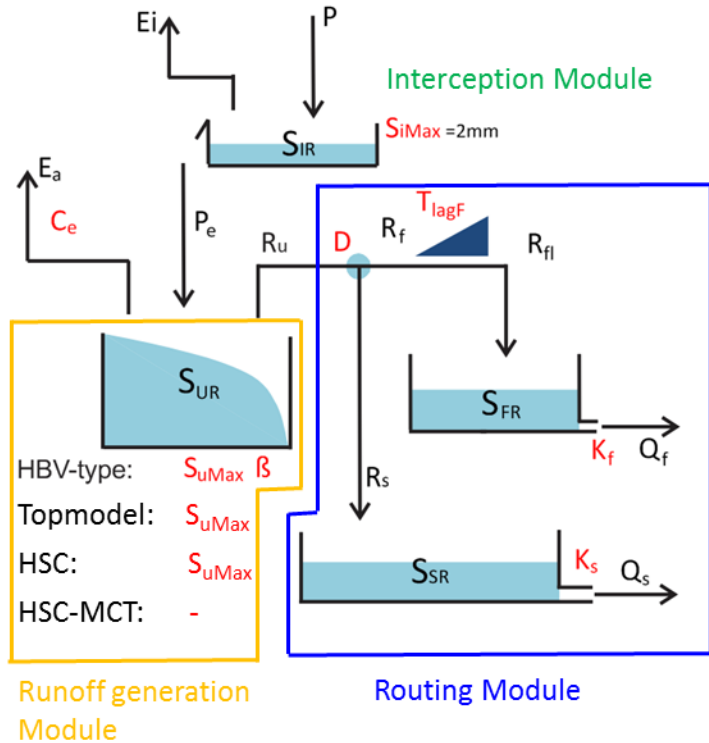
1257



1258

1259 Figure 34. The procedures estimating runoff generation by the HSC model and its two hypotheses.

1260



1261

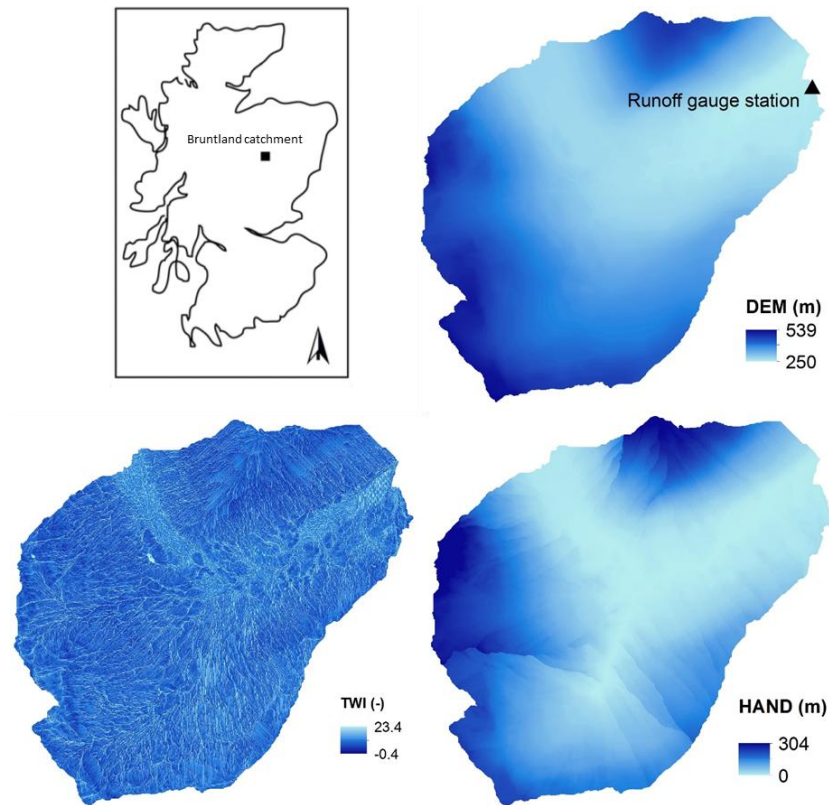
1262

1263 Figure 45. Model structure and free parameters, involving four runoff generation models (HBV-type, TOPMODEL,

1264 one free parameter; and HSC-MCT model does not have free parameter. In order to simplify calibration process and  
1265 make fair comparison, the interception storage capacity ( $S_{i\text{Max}}$ ) was fixed as 2mm.

1266

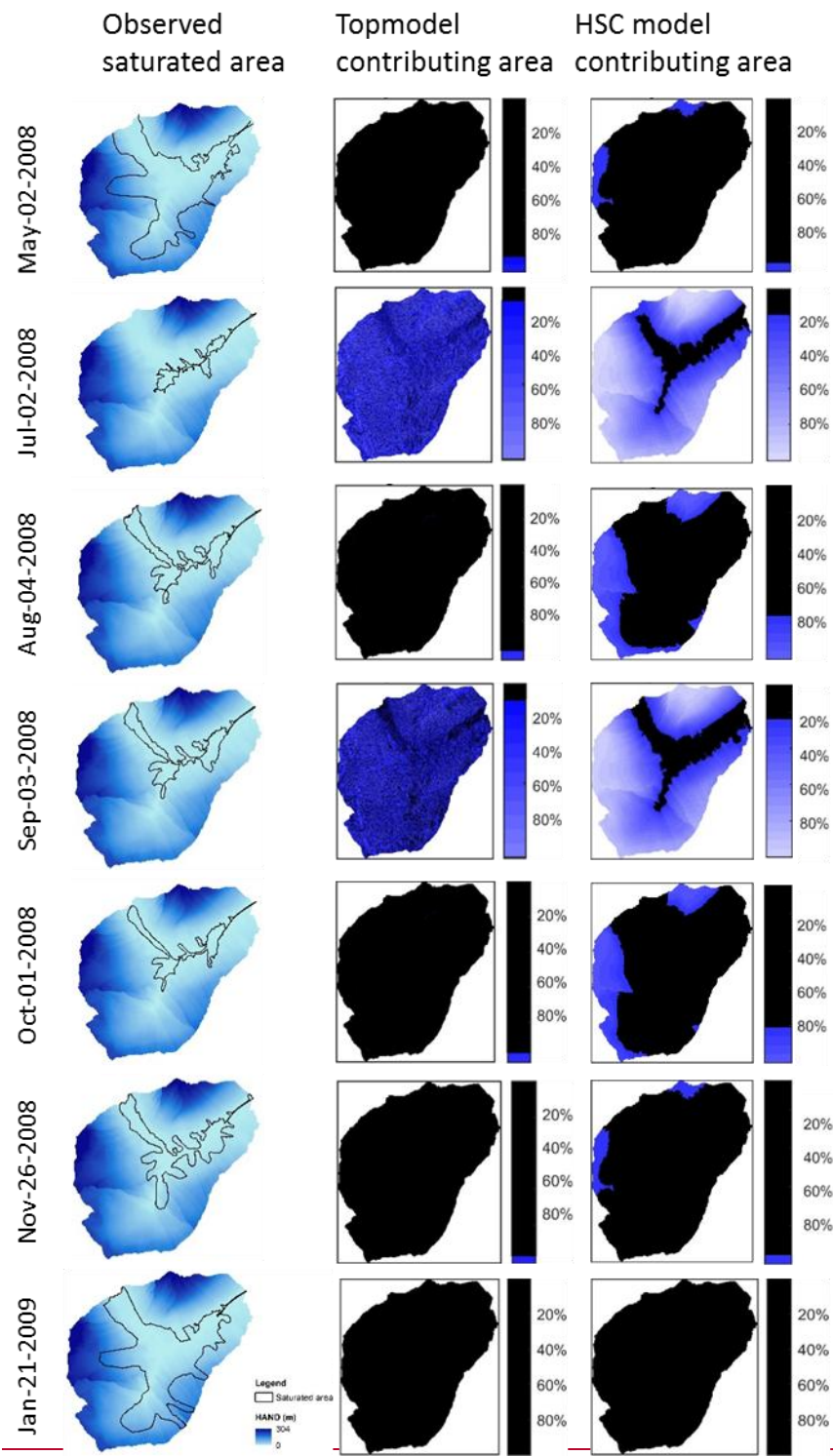
1267

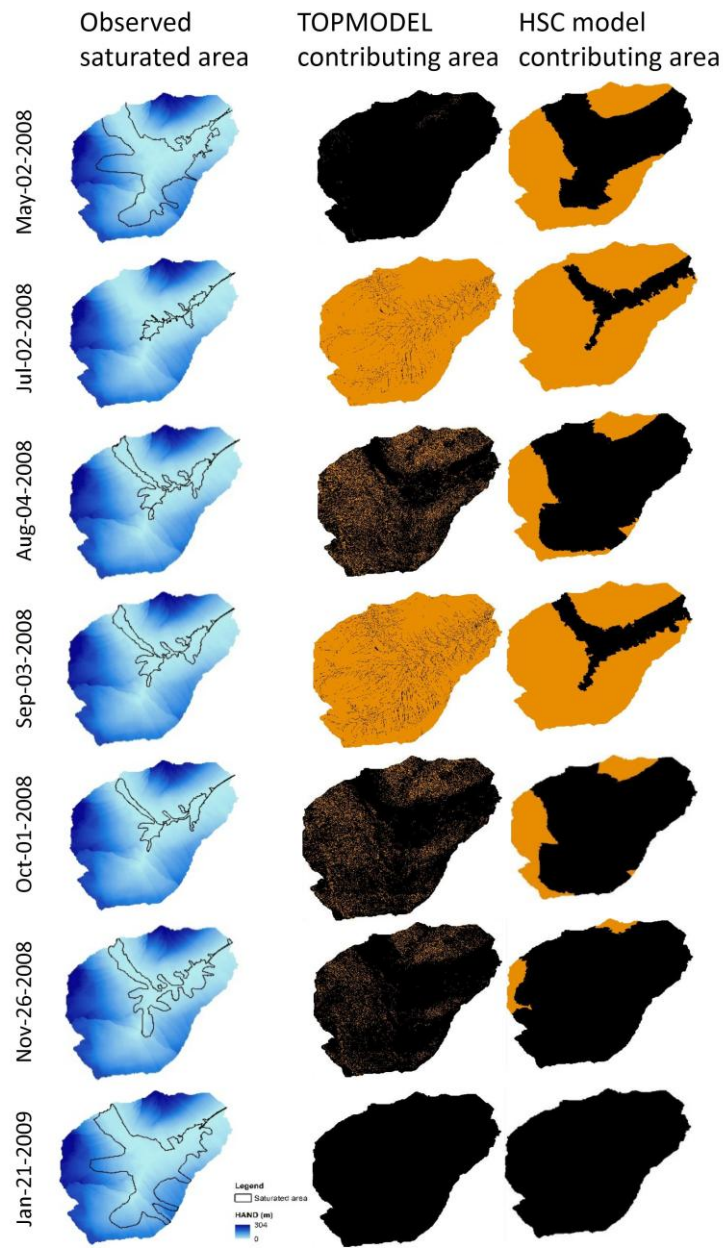


1268

1269 Figure 56. (a) Study site location of the Bruntland Burn catchment within Scotland; (b) digital elevation model (DEM)  
1270 of the Bruntland Burn catchment; (c) the topographic wetness index map of the Bruntland Burn catchment; (d) the  
1271 height above the nearest drainage (HAND) map of the Bruntland Burn catchment.

1272

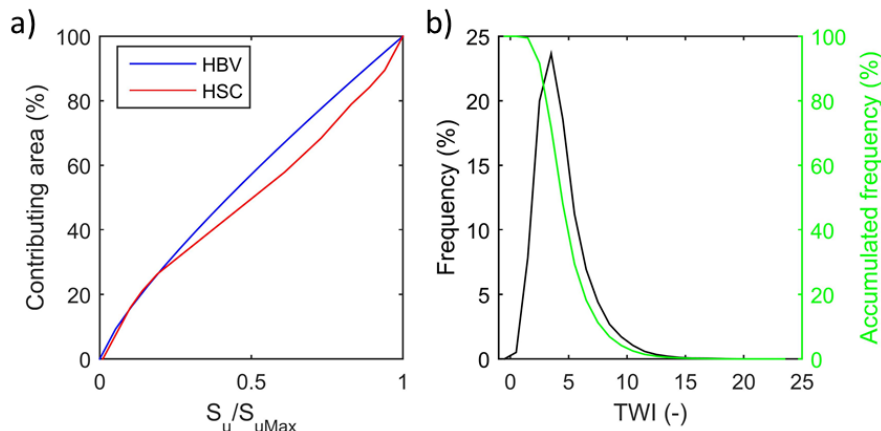




1274  
1275 Figure 67. The measured saturated areas and the simulated contributing areas black by TOPMODEL and HSC  
1276 models.

1277

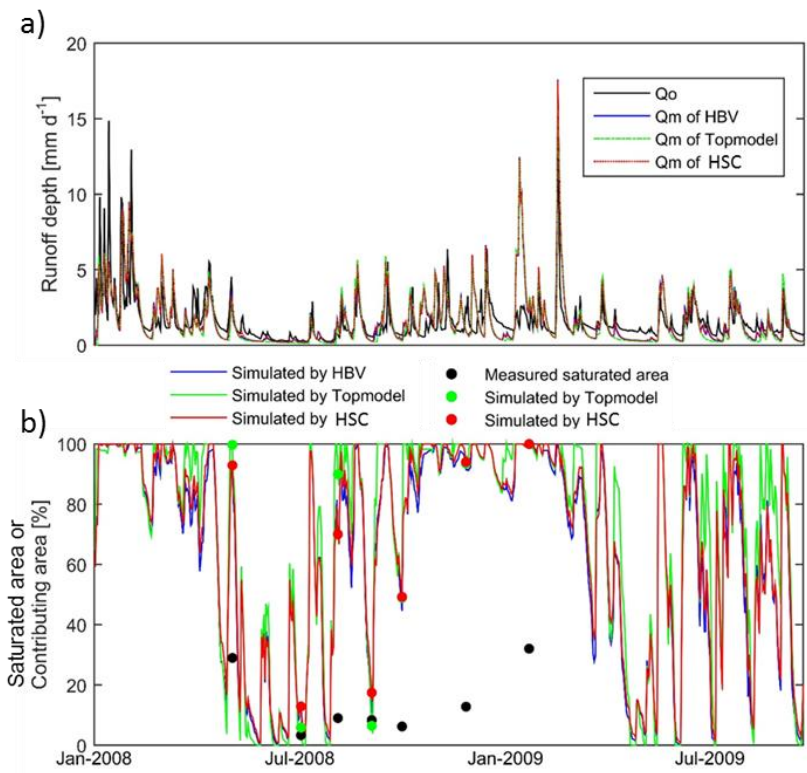
1278



1279

1280 Figure 78. The curves of the beta function of HBV model, and the  $S_u$ - $A_s$  curve generated by HSC model (the left figure).  
 1281 The frequency and accumulated frequency of the TWI in the Bruntland Burn catchment (the right figure).

1282

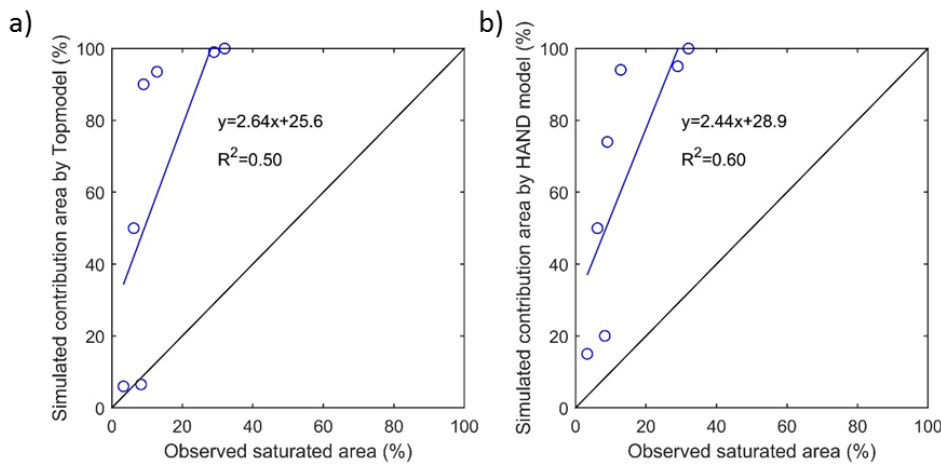


1283

1284 Figure 98. a) The observed hydrograph ( $Q_o$ , black line) of the Bruntland Burn catchment in 2008. And the simulated  
 1285 hydrographs ( $Q_m$ ) by HBV model (blue line), TOPMODEL (green dash line), HSC model (red dash line); b) the  
 1286 comparison of the observed saturated area of 7 days (black dots) and simulated relative soil moistures, i.e. HBV (blue  
 1287 line), TOPMODEL (green line and dots), HSC (red line and dots).

1288

1289



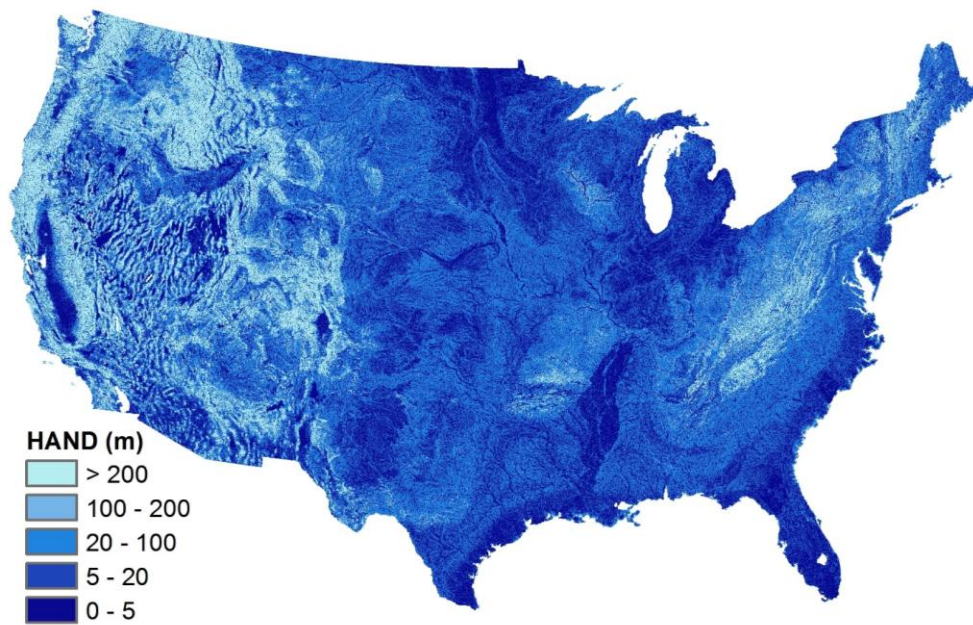
1290

1291 Figure 109. The comparison of the observed saturated area and simulated contributing areas by TOPMODEL and  
1292 HSC models.

1293

1294

1295

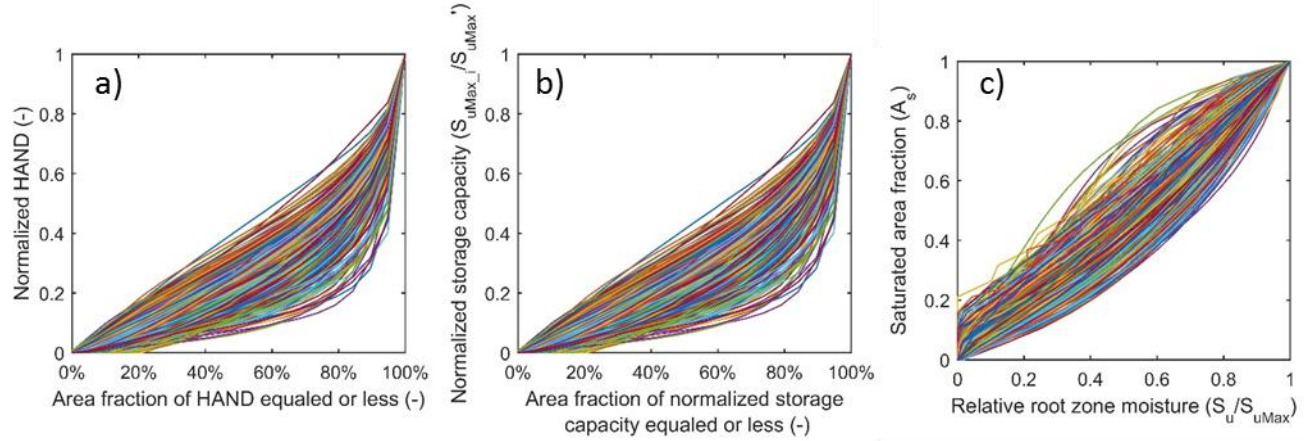


1296

1297 Figure 101. The Height Above the Nearest Drainage (HAND) map of the CONUS.

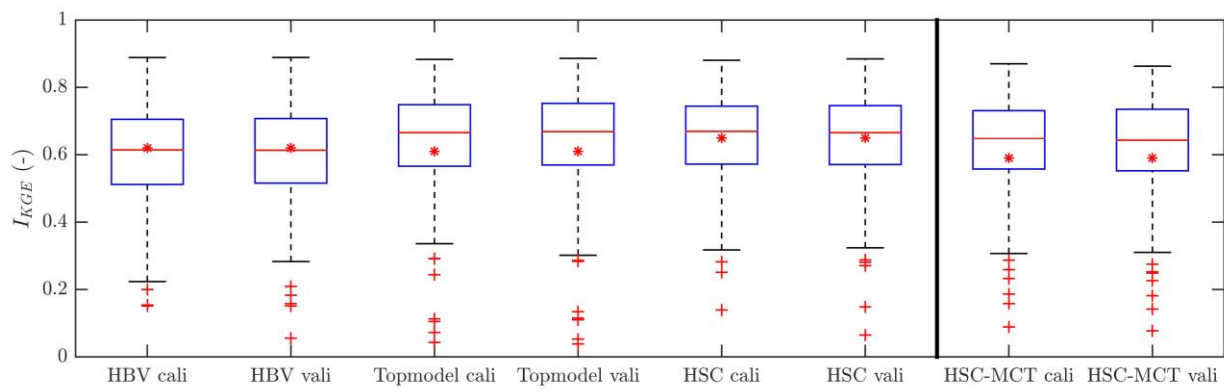
1298

1299



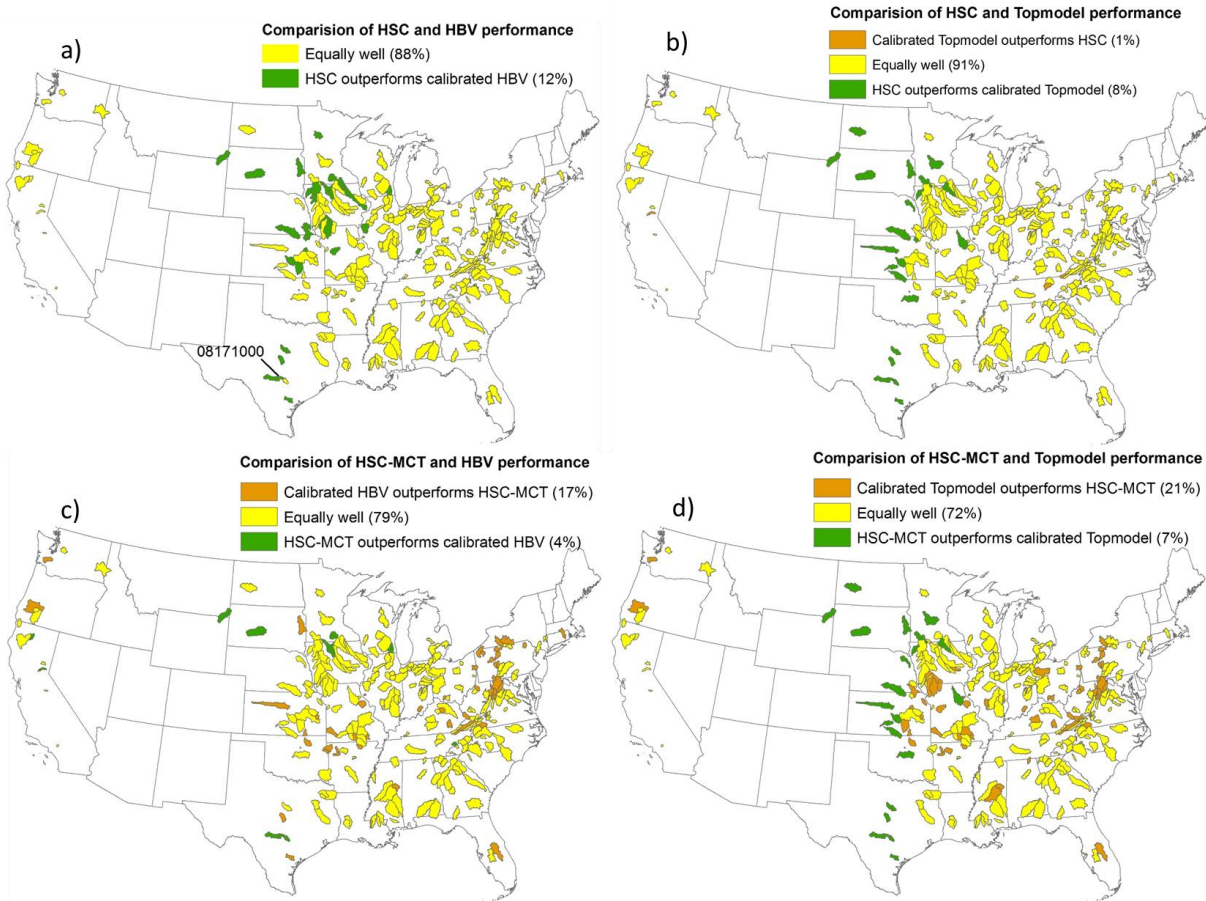
1300

1301 Figure 142. a) The profiles of the normalized HAND of the 323 MOPEX catchments; b) the relations between area  
 1302 fraction and the normalized storage capacity profile of the 323 MOPEX catchments; c) the  $S_u$ - $A_s$  curves of the HSC  
 1303 model which can be applied to estimate runoff generation from relative soil moisture for the 323 MOPEX catchment.  
 1304



1305

1306 Figure 123. The comparison between the HBV, the TOPMODEL, the HSC, and the HSC-MCT models  
 1307



1308

1309 Figure 134. Performance comparison of the HSC and HSC-MCT models compared to two benchmarks models: HBV  
 1310 and TOPMODEL, for the 323 MOPEX catchments.